TEXAS TECH UNIVERSITY
Multidisciplinary Research in Transportation

FRP Reinforcing Bars in Bridge Decks Field Instrumentation and Short-Term Monitoring

R. Scott Phelan
W. Pennington Vann
Jacob Bice

Texas Department of Transportation

Research Report 9-1520-04

August 2003

NOTICE

The United States Government and the State of Texas do not endorse products or manufacturers. Trade or manufacturers' names appear herein solely because they are considered essential to the object of this report

TECHNICAL REPORT DOCUMENTATION PAGE

1. Report No. FHWA/TX-06/9-1520-4	2. Government Accession No.	3. Recipient's Catalog No.
4. Title and Subtitle FRP Reinforcing Bars in Bridge Decks Field Instrumentation and Short-Term Monitoring		5. Report Date August 2003 6. Performing Organization Code TechMRT
7. Author(s) R. Scott Phelan, W. Pennington Vann, Jacob Bice		8. Performing Organization Report 9-1520-4
9. Performing Organization Name and Address Texas Tech University Department of Civil Engineering Box 41023 Lubbock, Texas 79409-1023		10. Work Unit No. (TRAIS) 11. Contract or Grant No. 9-1520
12. Sponsoring Agency Name and Address Texas Department of Transportation Research and Technology P.O. Box 5080 Austin, TX 78763-5080		13. Type of Report and Period Cover Technical Report, 9/1/01-8/31/03 14. Sponsoring Agency Code

15. Supplementary Notes
Study Conducted in cooperation with Texas Department of Transportation, Texas A&M University, and the University of Texas at Arlington. Research Project Title: "FRP Reinforcing Bars in Bridge Decks – Instrumentation and Monitoring"

16. Abstract:
Several types of instrumentation were installed by Texas Tech University on the Sierrita de la Cruz Creek bridge, located near Amarillo, Texas, for comparison of the performance of two spans with GFRP reinforcing bars in the top mat of the concrete deck to the performance of the other decks reinforced entirely with epoxy-coated steel (ECS). Short-term tests that were conducted included temperature measurements in the deck during and after a pour, crack mapping under no load and under static live loading, and deflection and strain measurements under static live loading. "Corrosion bars" and different types of "witness bars" were also placed in the deck for possible long-term studies in the future. The GFRP-reinforced concrete decks showed very good short-term performance. Only temperature and shrinkage cracks were observed, even under load, and the stiffness was as great or greater than predicted for an 8-inch deck thickness.

17. Key Words Glass fiber reinforced polymers, Concrete, Bridge, Deck, Corrosion Resistance, Field Instrumentation, Full-Scale Live Load Tests, Monitoring, Durability	18. Distribution Statement No restrictions. This document is available to the public through the National Technical Information Service, Springfield, Virginia 22161, www.ntis.gov.

19. Security Classif. (of this report) Unclassified	20. Security Classif. (of this page) Unclassified	21. No. of Pages 156	22. Price

Form DOT F 1700.7 (8-72)

FRP REINFORCING BARS IN BRIDGE DECKS
FIELD INSTRUMENTATION AND SHORT-TERM MONITORING

by

R. Scott Phelan, Ph.D, P.E.
W. Pennington Vann, Ph.D, P.E.
Jacob Bice, MSCE
Texas Tech University
Lubbock, Texas Tech University

Multidisciplinary Research in Transportation
Texas Tech University, Lubbock, TX 79409

Submitted to:
TEXAS DEPARTMENT OF TRANSPORTATION

Report 9-1520-4 Final Report August 2003

AUTHOR'S DISCLAIMER

The contents of this report reflect the views of the authors who are responsible for the facts and accuracy of the information presented herein. The contents do not necessarily reflect the official views or policies of the Texas Department of Transportation. This report does not constitute a standard, specification, or regulation.

PATENT DISCLAIMER

There was no invention of discovery conceived or first actually reduced to practice in the course of or under this contract, including any art, method, process, machine, manufacture, design or composition of matter, or any new useful improvement thereof, or any variety of plant which is or may be patentable under the patent laws of the United States of America or any foreign country.

ENGINEERING DISCLAIMER

Not intended for construction, bidding, or permit processes.

TRADE NAMES AND MANUFACTURERS' NAMES

The United States Government and the State of Texas do not endorse products or manufacturers. Trade or manufacturers' names appear herein solely because they are considered essential to the object of this report.

ACKNOWLEDGEMENTS

The authors would like to thank the project director, Tim Bradberry, who provided needed guidance and assistance. Special thanks go to the program coordinator, Ron Koester. Numerous other TxDOT personnel, including the project advisors, also took time to provide beneficial insights and information and we appreciate their help.

IMPLEMENTATION STATEMENT

The potential is high for information from this project to be used in the design of future concrete bridge decks for durability. The basic results from short-term tests performed with the installed instrumentation are that the two spans of the Sierrita de la Cruz Creek bridge reinforced in the top mat with glass fiber reinforced polymer (GFRP) bars performed very well. The observed surface cracking in the FRP-reinforced deck was due to temperature and shrinkage effects only, not load-induced, and the stiffness of the deck was greater than expected and essentially equal to that of the epoxy-coated steel (ECS) –reinforced deck.

Long-term monitoring can be pursued by various means with the instrumentation now available at the Sierrita de la Cruz Creek bridge. If this monitoring should indicate continued good performance of the FRP-reinforced deck, this method of avoiding corrosion damage to concrete bridge decks may see widespread implementation.

SI* (MODERN METRIC) CONVERSION FACTORS

APPROXIMATE CONVERSIONS TO SI UNITS

Symbol	When You Know	Multiply By	To Find	Symbol
	LENGTH			
in	inches	25.4	millimeters	mm
ft	feet	0.305	meters	m
yd	yards	0.914	meters	m
mi	miles	1.61	kilometers	km
	AREA			
in^2	square inches	645.2	square millimeters	mm^2
ft^2	square feet	0.093	square meters	m^2
yd^2	square yards	0.836	square meters	m^2
ac	acres	0.405	hectares	ha
mi^2	square miles	2.59	square kilometers	km^2
	VOLUME			
fl oz	fluid ounces	29.57	milliliters	mL
gal	gallons	3.785	liters	L
ft^3	cubic feet	0.028	cubic meters	m^3
yd^3	cubic yards	0.765	cubic meters	m^3
NOTE: Volumes greater than 1000 l shall be shown in m^3.				
	MASS			
oz	ounces	28.35	grams	g
lb	pounds	0.454	kilograms	kg
T	short tons (2000 lb)	0.907	megagrams (or "metric ton")	Mg (or "t")
	TEMPERATURE (exact)			
°F	Fahrenheit temperature	5(F-32)/9 or (F-32)/1.8	Celcius temperature	°C
	ILLUMINATION			
fc	foot-candles	10.76	lux	lx
fl	foot-Lamberts	3.426	candela/m^2	cd/m^2
	FORCE and PRESSURE or STRESS			
lbf	poundforce	4.45	newtons	N
lbf/in^2	poundforce per square inch	6.89	kilopascals	kPa

APPROXIMATE CONVERSIONS FROM SI UNITS

Symbol	When You Know	Multiply By	To Find	Symbol
	LENGTH			
mm	millimeters	0.039	inches	in
m	meters	3.28	feet	ft
m	meters	1.09	yards	yd
km	kilometers	0.621	miles	mi
	AREA			
mm^2	square millimeters	0.0016	square inches	in^2
m^2	square meters	10.764	square feet	ft^2
m^2	square meters	1.195	square yards	yd^2
ha	hectares	2.47	acres	ac
km^2	square kilometers	0.386	square miles	mi^2
	VOLUME			
mL	milliliters	0.034	fluid ounces	fl oz
L	liters	0.264	gallons	gal
m^3	cubic meters	35.71	cubic feet	ft^3
m^3	cubic meters	1.307	cubic yards	yd^3
	MASS			
g	grams	0.035	ounces	oz
kg	kilograms	2.202	pounds	lb
Mg (or "t")	megagrams (or "metric ton")	1.103	short tons (2000 lb)	T
	TEMPERATURE (exact)			
°C	Celcius temperature	1.8C + 32	Fahrenheit temperature	°F
	ILLUMINATION			
lx	lux	0.0929	foot-candles	fc
cd/m^2	candela/m^2	0.2919	foot-Lamberts	fl
	FORCE and PRESSURE or STRESS			
N	newtons	0.225	poundforce	lbf
kPa	kilopascals	0.145	poundforce per square inch	lbf/in^2

* SI is the symbol for the International System of Units. Appropriate

(Revised September 1993)

TABLE OF CONTENTS

List of Figures

List of Tables

EXECUTIVE SUMMARY

Fiber reinforced polymer (FRP) reinforcing bars are of interest as replacements for traditional black steel or epoxy-coated steel rebar in concrete bridge decks because of their resistance to corrosion. Corrosion of steel reinforcing bars in the deck has incurred high repair and replacement costs in concrete bridges, especially in locations susceptible to winter weather where de-icing chemicals are used. The Texas Department of Transportation (TxDOT), in cooperation with the Federal Highway Administration (FHWA), has initiated Research Project 9-1520 to design and construct a replacement for the seven-span Sierrita de la Cruz Creek bridge in the panhandle region of Texas with glass fiber reinforced polymer (GFRP) reinforcing bars in the top mat of two of the spans. The research effort has included FRP bar laboratory tests by researchers at Texas A&M University, consultations by researchers at the University of Texas at Arlington, and instrumentation and monitoring of the bridge by researchers at Texas Tech University. The bridge was designed by Timothy E. Bradberry, P.E., Senior Bridge Design Engineer at the TxDOT Bridge Division Office in Austin, Texas. This report documents the instrumentation and short-term monitoring performed by Texas Tech.

Several types of instrumentation were employed by Texas Tech on the Sierrita de la Cruz Creek bridge for comparison of the performance of the GFRP-reinforced concrete decks to the performance of the other decks reinforced entirely with epoxy-coated steel (ECS). Identical instruments were placed in the GFRP-reinforced Spans 6 and 7 and in the symmetric ECS-reinforced Spans 1 and 2, some for both short- and long-term studies and some for long-term studies only. The types of short-term measurement have included: 1) temperatures with thermocouples embedded in the deck; 2) cracking of the top surface of the deck, both with and without imposed loads; 3) displacements under load of the cantilevered edges of the deck relative to the exterior beams with displacement transducers (LVDT's) mounted on the beams (although these measurements were unsuccessful); 4) deflections under load at the centers of key spans with total station (surveying) instruments; and 5) strains under load with strain gauges embedded in the cast-in-place portions of the deck and surface-mounted on the precast deck panels and the supporting concrete beams. Any of these types of measurement can be repeated in the future, including the LVDT tests, to evaluate the long-term behavior of the decks with the two types of reinforcement. In addition, black steel "corrosion bars" were installed in the decks for future corrosion measurements, and black steel, ECS, and GFRP "witness bars" were installed near the top surface at several locations for possible extraction at intervals in the future so that the conditions of these three types of rebar can be examined and compared.

The short-term tests conducted by Texas Tech showed that the maximum internal deck temperature during the second phase of construction did not approach the levels at which the tensile strength and the bond strength of GFRP reinforcing bars have been found to be reduced. Also, the GFRP-reinforced spans showed very satisfactory performance under two sets of static live load testing: the cracking in the deck surface was all judged to be caused by temperature and shrinkage effects, none were identified as "load-induced," and the deflections and strains were less than theoretically predicted and comparable to those in the ECS-reinforced spans. It is recommended that the behavior of the bridge be monitored in the future with respect to cracking, corrosion measurements on the "corrosion bars," live load testing, and possibly extracting some of the "witness bars" for examination.

CHAPTER 1. INTRODUCTION

1.1 Background

Fiber reinforced polymer (FRP) reinforcing bars are of interest as replacements for traditional black steel or epoxy-coated steel rebar in concrete bridge decks because of their resistance to corrosion. Corrosion of steel reinforcing bars in the deck has long been one of the most costly problems with concrete bridges. Many concrete decks have required expensive repair and replacement procedures, especially in locations susceptible to winter weather where de-icing chemicals tend to accelerate the corrosion process. Epoxy coating of the steel bars has provided some help, but its promise is somewhat questionable, partly because there tends to be a concentration of corrosion whenever small holes or nicks in the coating occur.

In Texas, the current standard design of a concrete bridge deck utilizes 4-inch-thick precast prestressed concrete deck panels for the lower half of the 8-inch-thick deck and the upper four-inch portion is cast-in-place and reinforced longitudinally and laterally with a mat of steel bars. It is this upper mat which tends to have corrosion problems when water and de-icing chemicals seep down through small surface cracks in the top concrete cover and affect the steel. When extensive corrosion occurs the top cover breaks up and the deck can rapidly deteriorate.

While the precast prestressed deck panels spanning between the longitudinal beams have worked very well over the years (they are even believed to be capable of carrying the design loads without the upper cast-in-place part of the deck), the reinforcing in the upper mat must help carry negative lateral moments over the beams and in the overhangs. The lateral top mat reinforcing is also important to the capability of the barriers to resist a crash by a vehicle.

Replacing the top mat steel in a bridge of this type with FRP bars raises several questions. While the corrosion resistance of the bars is a definite advantage for the durability of the deck, the bars' much lower modulus of elasticity (at least for the less expensive glass fiber reinforced polymers, or GFRP, used in this project), questionable bond properties, potential for long-term deterioration from in-situ moisture, heat, and alkalinity, and relatively high cost all deserve attention. It was for this reason that a research project involving the application of FRP top mat reinforcement in an actual bridge replacement was initiated by the Federal Highway Administration (FHWA) and the Texas Department of Transportation (TxDOT) in August of 1999. The bridge in question was in Potter County in the panhandle of Texas, the part of the state where the winter weather is most severe. The project involved design and contract oversight from the TxDOT Bridge Division in Austin, construction by the Amarillo District of TxDOT, laboratory research and crash tests at Texas A&M University in College Station, consulting by an FRP expert at the University of Texas at Arlington, and field instrumentation and testing by researchers at Texas Tech University in Lubbock. This report summarizes the work carried out by the last group.

1.2 Object and Scope

The bridge designed and instrumented for this research was the Sierrita de la Cruz Creek bridge on State Highway 1061, approximately thirty miles northwest of Amarillo, Texas. It was in need of replacement because of structural deterioration and functional obsolescence. The new design called for seven spans of 79 feet each, as illustrated schematically in Figure 1.1, with the use of phased construction. The basic plan devised for studying the value of using FRP reinforcing bars in the top mat of the deck included placement of FRP bars in the two southern-most spans (Spans 6 and 7 in Figure 1.1) and the use of epoxy-coated steel (ESC) bars in the other five spans, including Spans 1 and 2, which would be symmetric with Spans 6 and 7. Thus a direct comparison could be made between the behavior of the two FRP-reinforced spans and that of the two steel-reinforced spans. Both short-term and long-term monitoring and testing of the bridge were envisioned.

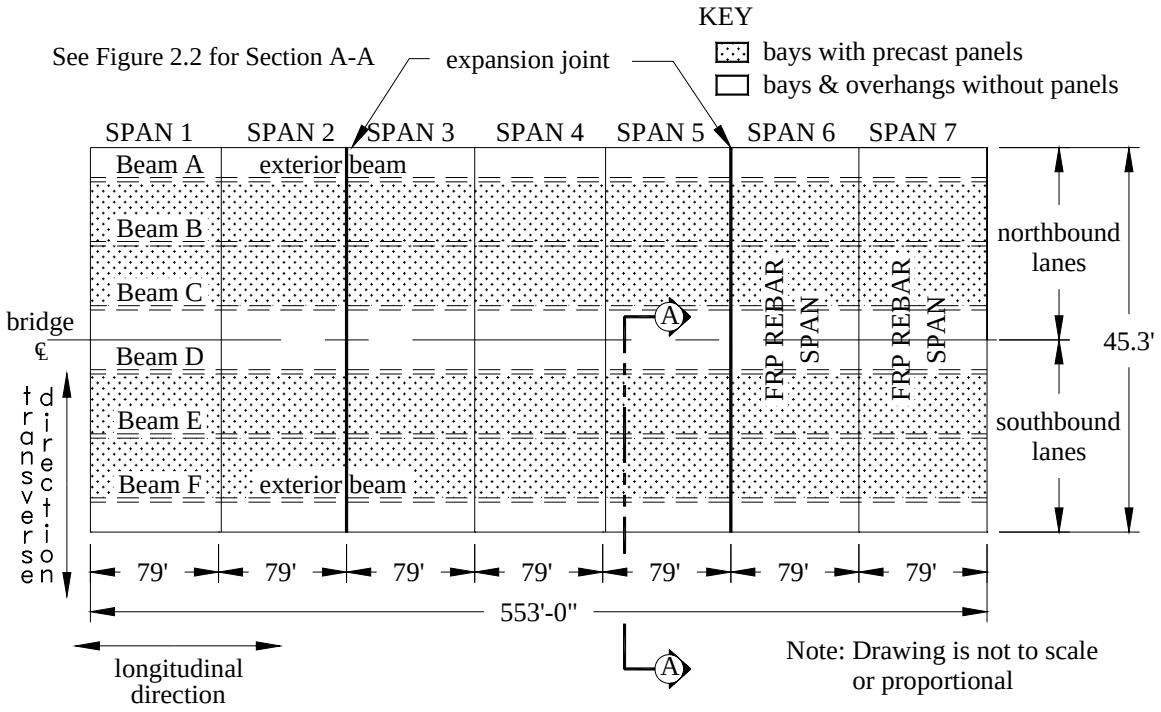

Figure 1.1 Plan View of the Sierrita de la Cruz Creek Bridge

The scope of the bridge instrumentation and related research included several elements, some aimed at short-term behavior and some at long-term behavior. First, it was decided to install an on-site weather station at the bridge that could be used to monitor basic weather parameters such as precipitation, air temperature, and humidity. Second, thermocouples were placed in the vicinity of one precast panel in each phase of the construction to monitor the temperature inside the upper cast-in-place (CIP) section of the deck during casting and afterward. Third, both internal and external strain gauges were placed at numerous strategic positions in Spans 1, 2, 6, and 7 to measure local strains under static live load testing. Fourth, mounting brackets for displacement transducers were installed to measure the displacements of the overhang edges relative to the outside beams. Fifth, measurement of absolute displacements using nearby surveying equipment was planned under live loading. Duplicate live load testing was

envisioned with monitoring of these strains and displacements in the FRP-reinforced and ESC-reinforced spans. Sixth, three black steel reinforcing bars were placed in each end of the bridge (and up into the adjacent barrier) during Phase I, with a wire connection to the outside for corrosion monitoring in the future, that is, to see how much corrosion would have occurred if black steel rebar had been used everywhere under the conditions experienced by the bridge. Finally, twelve sets of short "witness bars" were installed in the top of the CIP portion of the deck in different locations of Spans 1, 2, 6, and 7. These bars, which included three black steel, three epoxy-coated steel, and three FRP bars in each set, were intended for removal and examination at three later dates for further evaluation of the relative merits of the three types of reinforcement. Detailed drawings showing the locations of these bars are presented in Appendices A and B of this report so that the bars can be safely removed in the future.

The remaining sections of this chapter provide pertinent information about the Sierrita de la Cruz Creek bridge and the significance of this research. As further background relative to this research, a brief overview of FRP reinforcing bars and their application in concrete construction is presented in Chapter 2, along with comments about the advantages and disadvantages of this material. Chapter 3 presents the instrumentation carried out on the bridge, and Chapter 4 gives the procedures used in, and the results obtained from, two sets of live load tests carried out 13 months and 22 months after completion of the bridge deck, respectively. Finally, Chapter 5 summarizes the results of this study.

1.3 The Sierrita de la Cruz Creek Bridge

TxDOT's reconstruction of the Sierrita de la Cruz Creek bridge took place from January to December, 2000. The bridge is 553 ft (168.6 m) long and 45.3 ft (13.8 m) wide. As stated above, it consists of seven spans, each with five bays, and is supported by six prestressed concrete beams as shown in Figures 1.1 and 1.2. The supporting beams are TxDOT standard precast concrete type C I-beams and bear on the bridge bents with elastomeric bearing pads. The two spans at each end of the bridge (Spans 1 and 2 and Spans 6 and 7) are continuous with each other as well as symmetric with respect to the longitudinal centerline of the bridge.

The bridge was constructed in two phases with the northbound lanes being constructed first and the southbound lanes being constructed second. During the second phase a full-depth center bay slab was cast in place (see the left bay of Figure 1.2) to tie the new construction to the old. The other four bays of the bridge deck used 7'-2 ¼" (2.19-m) by 8-ft (2.4-m) precast prestressed concrete deck panels for the bottom four inches (100 mm) and cast-in-place concrete with top mat reinforcement for the top four inches (see the two 7'-10 ½" (2.4-m) bays of Figure 1.2). The outside cantilever parts of the deck were also cast in place, as shown in this figure. For the two spans with FRP top mat reinforcement, the bottom mats were epoxy-coated steel as in the top and bottom mats of the other spans of the bridge.

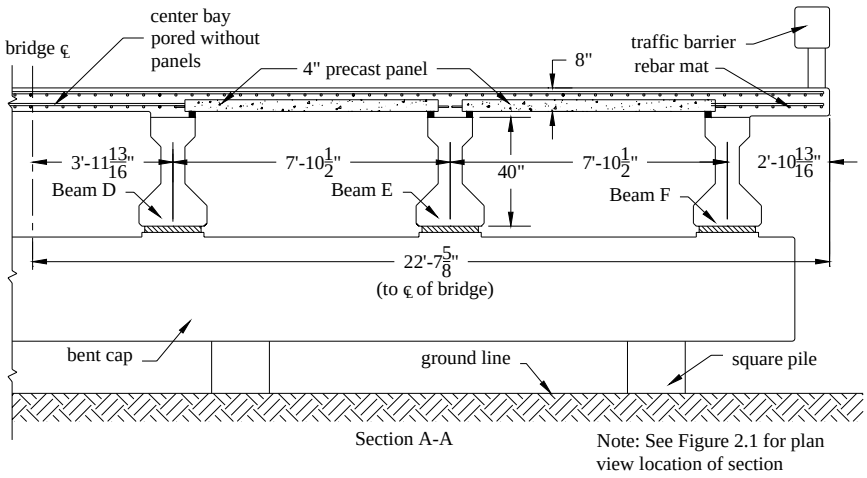

Figure 1.2 Typical Cross Section of the Bridge Deck

The top mats in Spans 6 and 7 of the bridge were reinforced with No. 5 and No. 6 Hughes Brothers Aslan 100 GFRP rebar with a nominal fiber content of 70% by volume (Hughes Brothers 2002). As shown in Figure 1.3, these bars have embedded sand and helical wrapping surface treatments for bond to the surrounding concrete. In the steel-reinforced spans, the top mat had No. 4 bars at a spacing of 9 inches in the longitudinal direction of the bridge and No. 5 bars at a spacing of 6 inches in the lateral direction. In the corresponding GFRP-reinforced spans, No. 5 Aslan 100 bars were spaced at 6 inches in the longitudinal direction and No. 6 Aslan 100 bars were spaced at 5.5 inches in the lateral direction. The GFRP combinations could be considered to be more than equivalent to the steel combinations for strength. However, in both directions the GFRP reinforcement provided only about one-half to two-thirds as much stiffness. This was due to the much smaller modulus of elasticity of the GFRP, as discussed further in Chapter 2. Table 1.1 compares the four rebar types and spacings on an equivalent stiffness (i.e., *E*A*) basis. It should be noted that because of the flexibility of the GFRP bars the top mat reinforcement was designed on the basis of stiffness and expected crack controlled, rather than strength. As a result, examination of the cracking in the top of the deck was given a high priority in the tests described in Chapter 4.

The reinforcement in the barriers of the Sierrita de la Cruz Creek bridge was designed to be epoxy-coated steel in all spans, both for the starter bars embedded in the deck and for the remaining steel above the deck. While corrosion at the deck/barrier interface is known to be a problem in bridges of this type, TxDOT bridge engineers did not believe that the barrier reinforcement could be changed to FRP without additional research, including crash tests to be conducted at Texas A&M University.

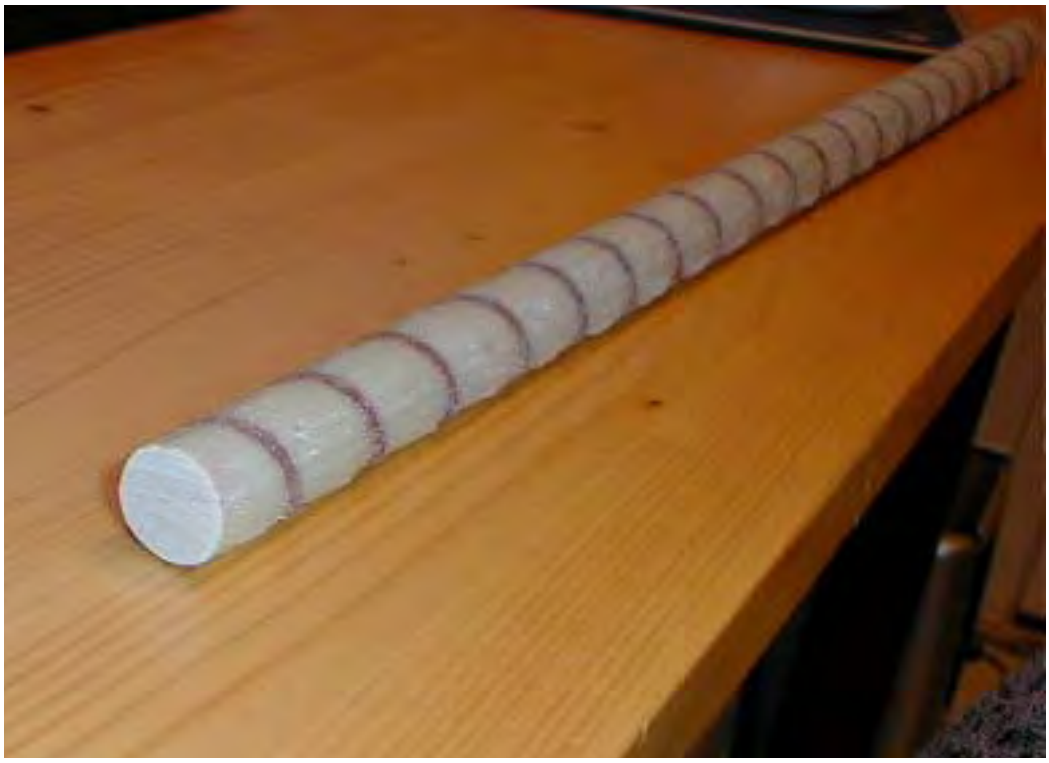

Figure 1.3 Hughes Brothers Aslan 100 GFRP Bar Sample

Table 1.1 Equivalent Axial Stiffnesses of Steel and GFRP Bar Combinations

Material	**Nominal Longitudinal Bar Size**	**Nominal Transverse Bar Size**	**Bar Spacing (in.)**		**Equivalent Axial Stiffness[1] (*E*A*), kips × 10^6**	
			Long.	**Trans.**	**Long.**	**Trans.**
Steel	4 (1/2" ϕ)	5 (5/8" ϕ)	9	6	5.7	17.8
Aslan GFRP	5 (5/8" ϕ)	6 (3/4" ϕ)	6	5.5	4.0	8.1

[1] For a one-foot wide section

1.4 Significance of the Research

While the Sierrita de la Cruz Creek Bridge is not the first bridge to be constructed using FRP reinforcing bars, it is unique in that it is the first of its kind in the State of Texas. In addition, since the ECS-reinforced Spans 1 and 2 are symmetrical with the FRP-reinforced Spans 7 and 6, as shown in Figure 1.1, a direct comparison of the relative performances of the two bridge deck systems is possible. Since an increased durability of the deck is the main reason for trying FRP reinforcement, studies of the bridge will be needed over an extended period of time. This report cannot provide the results of such studies, which hopefully will be conducted five, ten, and 30 years into the future. What this report does cover is the

instrumentation installed to allow for such studies and the results of a few short-term tests performed 13 and 22 months after the completion of the bridge.

The short-terms tests were aimed at evaluating two key aspects of the bridge's behavior: flexibility and cracking. These are considered to be related; if the FRP-reinforced deck is overly flexible because of the lower stiffness of the FRP bars, it will be more susceptible to load-induced top surface cracking, especially in the negative moment regions over the beams and in the overhangs. Such cracking, in turn, may allow penetration of de-icing salts to a greater depth in the bridge deck than in a deck with ECS in the top mat, potentially even to the depth of the steel reinforcement in the bottom mat. The prestessed steel in the precast panels would not likely be affected by this penetration, but the bottom mat rebar in the overhang and in the full-depth cast-in-place middle bay could be affected. If cracking were to reach the depth of the non-prestressed bottom mat reinforcement, corrosion of this steel could proceed at a rapid rate, and the service life of the bridge could be significantly reduced. Thus, a greater flexibility of the bridge deck could potentially negate the positive aspects of the electrochemically inert nature of the FRP.

Even if top surface cracks did not penetrate to the depth of the bottom mat reinforcement, cracking of the bridge deck could degrade its ride quality and necessitate excessive and early maintenance of the deck. In this case, an increased flexibility of the bridge deck could potentially negate the FRP bars' advantage of increased economy through better life cycle costs by increasing the amount of maintenance required on the bridge deck. With these considerations in mind, the relative flexibilities of the FRP- and ECS-reinforced decks, as measured during load tests, and the cracking behavior, as evaluated through crack mapping, should be significant contributions to the understanding of FRP reinforcement in concrete bridge decks.

Other short-term studies on the Sierrita de la Cruz bridge that could provide useful insights include the temperature measurements taken during casting and the related weather data collected simultaneously.

With regard to monitoring the long-term durability of the FRP- and ECS-reinforced decks in the Sierrita de la Cruz Creek bridge, several significant capabilities have been incorporated into the instrumentation. First, thermocouples have been placed in the deck, and they could be combined with a reactivated weather station to evaluate the long-term temperature stresses placed on the FRP bars. Second, long black steel "corrosion bars" placed in the deck and bent up into the barrier are available for testing of the rate of corrosion that would be taking place in the deck if uncoated steel had been used. This information should provide a benchmark for considering the value of both ECS and FRP reinforcement in the particular environment of this bridge. Finally, the short "witness bars" placed in both the FRP- and ECS-reinforced spans can be extracted from the decks at different times and examined to see how well the different types of bars (black steel, epoxy-coated steel, and GFRP) have fared over time. Extractions after three, ten, and 30 years are recommended.

CHAPTER 2. FIBER-REINFORCED POLYMER BARS

2.1 Overview

Fiber reinforced polymers are defined as fibers, natural or synthetic, encased in a polymer matrix. The polymer used can either be a thermosetting polymer or a thermoplastic polymer to fit the general definition of FRP. However, according to Canadian bridge design provisions for use of FRP as reinforcement in concrete, only thermosetting polymers are to be used for the polymer matrix. Thermosetting polymers have displayed superior performance characteristics to those of thermoplastic polymers (Bahkt et al, 2000).

Fibers used in construction are typically either glass, aramid, or polyactrinitrile-based (PAN) carbon fibers. FRP bars used as reinforcement in concrete bridge decks are manufactured by "pultrusion." Pultrusion is a continuous process for manufacturing composites that have a uniform cross-sectional shape. The process consists of pulling a fiber-reinforced material through a resin impregnation bath, then through a shaping die where the resin is subsequently cured. Surface treatments may be applied to a pultruded bar, such as embedded sand, surface deformations, helical wrapping, or a combination of embedded sand and helical wrapping. Surface treatments are used to increase the mechanical bond between the concrete and the FRP bar (see Figure 1.3).

2.2 Mechanical Properties of FRP

Glass FRP bars were used in the Sierrita de la Cruz Creek bridge. These bars typically have a tensile strength between 70 and 230 ksi and an elastic modulus between 5,100 and 7,400 ksi, as shown in Table 2.1. However, Hughes Brothers, Inc., specifies tensile strengths of 95 ksi and 90 ksi and a common modulus of elasticity of 5,920 ksi for No. 5 and No. 6 Aslan 100 GFRP bars, respectively (Hughes Brothers, 2002). Aramid fibers have tensile strengths between 250 and 368 ksi and elastic moduli between 6,000 and 18,200 ksi. PAN-based carbon fibers have tensile strengths between 87 and 535 ksi and elastic moduli between 15,900 and 84,000 ksi (ACI 440, 2001). These properties are summarized in Table 2.1. It should be noted, however, that while certain types of FRP material display superior mechanical properties to those of steel, the cost of using some types of FRP, such as PAN-based CFRP, typically is prohibitive.

Table 2.1 Mechanical Properties of FRP Bars

	Steel[a]	GFRP[b]	Aslan 100 GFRP[c]	CFRP[b]	AFRP[b]
Nominal Yield Stress, ksi	40-75	N/A	N/A	N/A	N/A
Tensile Strength, ksi	60-100	70 to 230	90 to 95	87 to 535	250 to 368
Elastic Modulus, × 10^3 ksi	29	5.1 to 7.4	5.92	15.9 to 84.0	6.0 to 18.2
Yield Strain, %	2.1 to 2.6	N/A	N/A	N/A	N/A
Rupture Strain, %	6.0 to 12.0	1.2 to 3.1	--	0.5 to 1.7	1.9 to 4.4

[a] ASTM A615/ASTM 615M-1b
[b] ACI 440 2001
[c] www.hughesbros.com/mechprop.html 9/19/2002

As shown in Table 2.1, fibers can have wide ranges of mechanical properties. These differences are due to variations in raw materials and fabrication methods. PAN-based carbon fibers, which exhibit the greatest amount of variation in mechanical properties, vary in accordance with the heat of carbonization of the carbon fibers (Riggs, et al, 1982). The higher the heat of carbonization, the greater the ultimate tensile strength and the elastic modulus of the fiber. However, increased heat of carbonization also directly affects the cost of manufacturing the PAN-based carbon fibers. These fibers are by far the most expensive to produce of those listed in Table 2.1.

2.3 Advantages and Disadvantages

The primary advantage of, and therefore the incentive to use, FRP bars as reinforcement in concrete bridge decks is their resistance to corrosive elements typically found in concrete from the application of de-icing salts. FRP bars have a high tensile strength, typically on the order of two times that of steel for GFRP fibers and as much as five times that of steel for carbon fibers (ACI 440, 2001). However, the high tensile strength advantage of the glass FRP is limited by its relatively low modulus of elasticity and lack of yielding before brittle rupture (ACI 440, 2001). Individual batches of FRP bars can vary in strength from one batch to the next. Thus, it is necessary to test each batch of bars for tensile capacity.

Additional advantageous properties of FRP bars are their light weight (typically a quarter of the density of steel) and low thermal and electrical conductivities (ACI 440, 2001). The nonconductive nature of FRP bars is of particular interest as this property makes FRP reinforcement impervious to the galvanic corrosion phenomena to which steel reinforcement is susceptible.

2.4 Use of FRP Bars in Concrete

Standard practice in steel-reinforced concrete design is to “under-reinforce” the structure so that the reinforcing steel yields before the concrete fails. This design philosophy provides steel-reinforced concrete structures with a ductile failure mode that gives warning to engineers. While a sudden catastrophic failure of a GFRP-reinforced structure is possible if it is improperly designed, a properly designed GFRP-reinforced concrete section actually has a good amount of deformability prior to failure. This result comes about because the section is designed for cracking of the concrete and the low modulus of elasticity of the GFRP keeps it well below its breaking strength at concrete cracking strains. Then the GFRP stretches to a large strain before failure. Certain carbon fiber-reinforced polymer (CFRP) bars, in contrast, have a modulus of elasticity similar to that of steel (see Table 2.1), so the full capacity of CFRP bars can be utilized in concrete sections. This feature typically results in a smaller amount of CFRP reinforcement for a bridge deck when a sufficient stiffness is achieved. A ductile failure for carbon bars has been proposed (Phelan 1993), but cost is a determining factor for CFRP. For this research project only glass FRP was considered.

Typically, steel reinforcement in concrete bridge decks is designed simply to provide sufficient capacity to resist the anticipated loads. The relatively high stiffness of steel resists cracking of the deck when it is designed for such strength control. The low modulus of

elasticity of FRP bars, on the other hand, does not allow bridge designers to fully utilize the strength of the FRP material, since limiting cracking in the deck typically governs the design of the reinforcement.

2.5 Degradation of GFRP Bars

The designer of the Sierrita de la Cruz Creek Bridge noted several additional challenges involved in the design of the bridge using FRP bars (Bradberry, 2001). The first of these challenges was that glass and aramid fibers can be subjected to attack by acidic and caustic solutions if the protection of the polymer matrix is inadequate. The caustic environment of wet concrete can penetrate through polymer matrices and degrade glass and aramid fibers. Independent tests showed that immersion of GFRP bars for two months in a lime solution with a pH value of 13 reduced the tensile strength by thirty percent and the elastic modulus by fifty percent (Soroushian, et al, 2001). However, this research was performed at an elevated temperature (60°C or 140°F) not likely to be achieved in an actual bridge deck. Also, Soroushian did not use a polymer matrix similar to the one used in the Sierrita de la Cruz Creek bridge. Nevertheless, researchers continue to be in disagreement as to the durability of these fibers in a wet concrete environment (Bradberry, 2001). The GFRP bars used in this research utilize a vinyl-ester-based polymer. This type of polymer has been shown to have a better durability than epoxy-based polymers in the wet concrete environment (ACI 440, 2001). The measures provided for long-term monitoring of the durability of the FRP bars in the Sierrita de la Cruz Creek bridge are presented in detail in Chapter 3 of this report.

2.6 Shear Strength

FRP bars have low shear strengths compared to their tensile capacities (Bradberry, 2001). This weakness is due to the orthotropic nature of pultruded FRP bars, unlike the isotropic nature of steel bars. Thus, steel bars are able to contribute dowel action to the shear capacity of a bridge deck. The shear strength of FRP bars typically is governed by the strength of the polymer matrix which surrounds the fibers. Thus, FRP bars cannot be considered to contribute significant dowel action to the shear capacity of a concrete bridge deck. This aspect is of particular concern in the overhang sections of the deck.

2.7 Lateral Coefficient of Thermal Expansion

Due to the relatively large radial coefficient of expansion of FRP bars, spalling may occur if the concrete cover is insufficient (Bradberry, 2001). Table 2.2 shows a larger coefficient of thermal expansion for GFRP bars than for steel bars in the transverse direction: 6.5×10^{-6}/°F for steel bars and between 11.7 and 12.8×10^{-6}/°F for GFRP bars (ACI 440, 2201). Numerical analysis has also shown that radial thermal expansion of FRP bars may cause cracking of the surrounding concrete, which could affect the bond of the FRP bars to the concrete (Gentry, 1999). Bond between FRP bars and concrete has been observed to be developed by a combination of adhesion of the concrete to the bar, friction between the bar and the concrete, and mechanical interlocking of the concrete with either the embedded sand surface treatment or indentations created by helical wrappings (Katz, 2000). Cracking of the surrounding concrete due to thermal expansion may cause a loss of the mechanical

interlocking action between the bar and the concrete. On the other hand, the helical wrapping may restrict the thermal expansion (Gentry, 1999). Katz (1998) also notes that this restriction may cause damage to the longitudinal fibers in the FRP bar.

Table 2.2 Coefficients of Thermal Expansion[1]

Direction	Coefficient of Thermal Expansion ($\times 10^{-6}$/°F)				
	Concrete	Steel	GFRP	CFRP	AFRP
Longitudinal, α_L	5.5	6.5	3.3 to 5.6	-4.0 to 0.0	-3.3 to -1.1
Transverse, α_T	5.5	6.5	11.7 to 12.8	41 to 58	33.3 to 44.4

[1] Source: ACI 440 (2001)

2.8 Water Absorption and Elevated Temperatures

GFRP has been found to be susceptible to water absorption, which can cause fairly large volumetric changes in the bars. These volumetric changes can cause stresses to be induced in the surrounding concrete, and, in turn, crack the surrounding concrete. Again, should the concrete around an FRP bar become cracked, the bond of the bar to the concrete may be significantly reduced (Cosenza, 1997). Research by Nishizaki and Meiarashi (2002) has also found that the tensile strength of GFRP is deteriorated by immersion in a wet environment. Cracks were found to emerge on the surfaces of the GFRP specimens and the weight of the specimens decreased during testing, indicating a loss of tensile capacity. This research suggests that the GFRP in the Sierrita de la Cruz Creek bridge deck could be susceptible to deterioration simply due to its moist concrete environment during casting. While most of the testing of Nishizaki and Meiarashi occurred at elevated temperatures, some deterioration did occur at a temperature of 40°C (104° F). This temperature is well within the range of temperatures experienced by the Sierrita de la Cruz bridge deck during the summer months. Thus, the internal temperature of the deck was monitored as a part of this research, as discussed in Chapters 3 and 4. It should also be noted that a 100% vinyl ester resin was used in the Aslan 100 bars to reduce the absorption potential of the bars.

Bond of GFRP bars to concrete is primarily dependent on the polymer matrix. Elevated temperatures also reduce the bond of the bars. However, research performed by Katz, et al (1999) showed that a large reduction in bond strength was not seen until temperatures were elevated to a range between 180 and 200°C (356 and 392°F), which is outside the range of temperatures expected to be experienced by the Sierrita de la Cruz Creek bridge deck. This temperature range is also significantly higher than the temperatures at which Nishizaki and Meiarashi (2002) began to observe a reduction in tensile strength of GFRP bars. Therefore, it is likely that a reduction in the tensile strength of the GFRP bars would occur well before a significant loss of bond strength due to temperature.

2.9 Surface Treatments on FRP Bars

Steel bars develop bond with the surrounding concrete primarily through mechanical interaction between lugs on the bars and the concrete. Similarly, FRP bars develop bond with

the concrete through interaction between various surface treatments on the bars and the concrete. The bars used in the Sierrita de la Cruz Creek bridge deck utilize both an embedded sand surface treatment and a helical wrapping to increase the bond with the concrete. Katz (1998) has shown that cyclic loading of FRP bars with helical wrappings has the potential for premature failure due to transverse pressure induced on the glass fibers in the bars by the helical wrapping. However, this phenomenon can be avoided with proper design of the helical wrapping (Katz 1998). While the bars used in the Sierrita de la Cruz Creek bridge have the appropriate wrapping, it is of interest to know if the cyclical loading experienced by the bridge over time will place these bars at risk due to transverse stresses induced by the helical wrappings. Extracted witness bars could assist in evaluating this concern.

2.10 Cost

FRP bars also incur a higher initial cost than steel reinforcement (Bradberry, 2001). Use of GFRP bars for the top mat of the entire Sierrita de la Cruz Creek Bridge would have increased the cost of the bridge by 6.4% as compared to the cost of a conventionally reinforced bridge deck. However, as pointed out by Hastak and Halpin (2000), when one considers the life-cycle cost associated with a bridge deck, the initial costs may be far outweighed by future savings in maintenance costs, operating costs, and disposal costs. Thus, if FRP bars can extend the service life of a bridge deck by increasing its resistance to freeze-thaw cycles and provide adequate stiffness to prevent load-induced cracking, substantial savings in maintenance and postponement of replacement can be realized.

CHAPTER 3. INSTRUMENTATION AND MEASUREMENTS

3.1 Measurement Categories

For the Sierrita de la Cruz Creek bridge, the research team developed a variety of measurement systems for evaluating both the short-term and long-term performance of the spans with fiber-reinforced polymer (FRP) reinforcement and with epoxy-coated steel (ECS) reinforcement. Generally the instrumentation was identical in the two ECS-reinforced spans (Spans 1 and 2) and the two FRP-reinforced spans (Spans 6 and 7). Some of the instrumentation was removed either during or at the end of the term of the research project; other elements were left in place for possible future use. The first types of short-term measurement consisted of ambient weather data and temperature readings from thermocouples mounted in the cast-in-place (CIP) part of the deck during casting. The second types of short-term measurement consisted of displacement and strain measurements, plus crack mapping exercises, during two live load tests. The long-term measurements hopefully will consist of: 1) corrosion rate readings on black steel bars put in the deck and barrier for this purpose; 2) examination of FRP, ECS, and black steel "witness bars" extracted from the deck; 3) later live load tests for comparison to the ones already completed; and 4) general observations of the condition of the bridge, especially with regard to the relative endurance of the two FRP-reinforced deck spans and the two symmetric ECS-reinforced spans.

This chapter documents the types of instruments used and their locations. More detailed figures showing where all the strain gauges, corrosion bars, and witness bars are positioned, how the crack mapping subareas are designated, and other information that will be needed for future users of the instrumentation system are shown in Appendices A and B. It should be noted that some of the instrumentation components discussed below have been taken out of service and other components were damaged by the construction crews or vandals to the point that they were found to be inoperable during the two sets of live load tests that were conducted. In addition, some channels of data were not recorded properly by the field-mounted data acquisition system during the live load tests, but the instruments themselves were not faulty. In discussing each category of instrumentation below, the inoperable components are identified in the hope that useful tests may be carried out in the future. Basically, the weather station has been taken out of service, some of the internal and external strain gages and their wires were damaged (Appendix D identifies which ones are still operable), data from the edge-mounted displacement transducers were improperly recorded but the mounting brackets are in place for future use, all of the corrosion bars with external wires are in place for future corrosion rate measurements, and all of the witness bars are in place for future extraction for examination and testing.

3.2 Weather and Deck Temperature Measurements

A portable tower for monitoring the climatic conditions at the bridge site was erected in July 2000 during the first phase of the construction. The tower instruments included temperature and humidity sensors, an anemometer to measure wind speeds, and a tipping bucket to measure precipitation. The weather tower is shown in Figure 3.1. Data from the instruments

were stored in a Campbell Scientific CR10X battery powered datalogger. Originally the contractor planned to supply A/C power and a phone line to the bridge. When these plans changed, TTU researchers modified the data acquisition procedure.

Figure 3.1 Weather Tower at Bridge Site

Specifically, a remote data acquisition strategy using a modem was abandoned. Also, battery power became necessary. The battery for the datalogger was kept charged by a solar panel installed on the weather tower. The datalogger had the capacity to record data from all of the weather instruments as well as the ten thermocouples placed in the first phase deck. These data could be recorded every half hour for a month without overwriting existing data.

Climatic data at the bridge site were of interest to measure the outside temperatures and other conditions during casting and to determine the number of freeze-thaw cycles experienced by the bridge. Furthermore, the difference between the ambient temperature and the temperature inside the bridge deck could be monitored. One measurement of ambient temperature was recorded by a thermocouple located underneath the bridge inside the junction box housing the datalogger. However, it should be noted that the temperatures measured by this instrument (beneath the bridge) were much lower than those inside the bridge deck. Temperature and weather conditions during casting are discussed in Section 4.3.

A set of thermocouples was installed in the cast-in-place deck of the Sierrita de la Cruz Creek bridge during both phases of construction. The main purpose of the thermocouples was to monitor temperatures inside the bridge deck as the heat of hydration developed. The thermocouples could also be used in the future to monitor the number and severity of freeze-thaw cycles experienced by the bridge deck. Figure 3.2 shows the locations of the thermocouples placed during the second phase of construction. Ten thermocouples were installed in a grid that was centered around a precast panel in Span 6 of the bridge. Six of the thermocouples were placed at the height of the top mat of reinforcement (i.e., at the midheight of the four-inch-thick CIP part of the deck), with four at the corners and two at the center of the panel. The other four thermocouples were placed at the height of the precast panel tendons (i.e., at the midheight of the lower four-inch-thick part of the deck), again at the corners of the panel. An identical arrangement was used in the first phase of the construction.

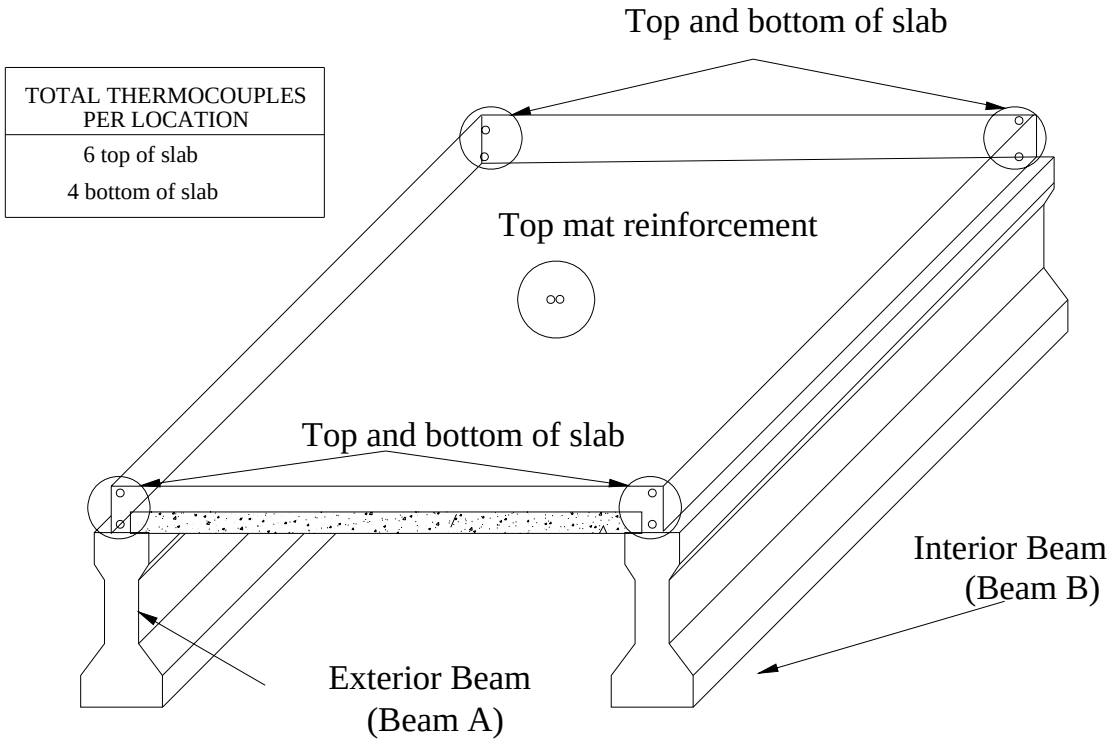

Figure 3.2 Thermocouple Locations Centered Around a Precast Panel

The weather station with its datalogger, battery, and solar panel for power was removed after construction crews cut the wires between the station and the datalogger during final grading of the site. However, the eight thermocouples inside the two Phase I and Phase II deck panels are still in place with their lead wires into the junction box under the bridge and they are operable.

3.3 Displacement Measurements

Two types of displacement measurement were envisioned for the live load tests on the FRP- and ECS-reinforced bridge segments. The first type consisted of linear variable displacement transducers (LVDT's) supported from the outside beams to record the deflections of the outside edges of the deck under load (see Figure 3.3). These relative displacements were expected to aid in understanding the behavior of the negative-moment cantilever portions of the deck where the top mat reinforcement would be of special importance and would differ from FRP to ECS.

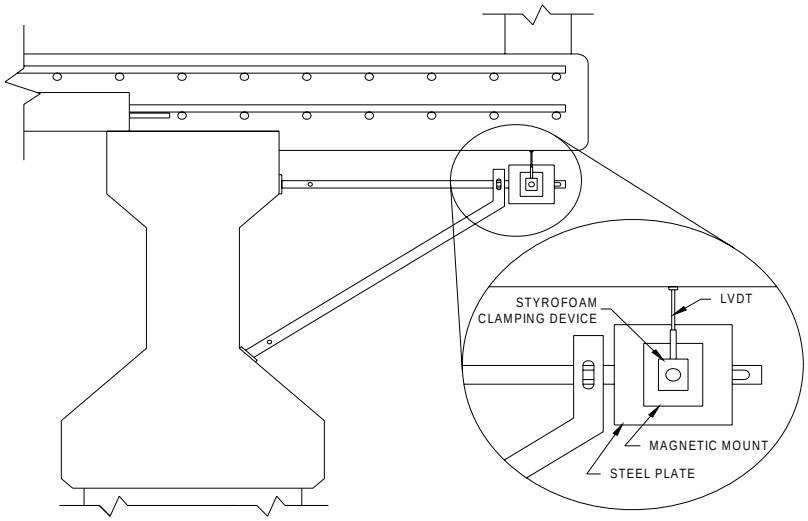

Figure 3.3 LVDT Mounted to Measure Overhang Displacements

It was expected that wheel loads placed as far out on the cantilevers as possible would provide useful data. The other type of displacement measurement consisted of total station (surveying) readings of deflections at the centerline of the bridge with loads placed near the centerline.

The installation of the LVDT's was successful during the first set of live load tests in December, 2001, but there was a malfunction of the data acquisition system module that should have recorded the data. While no data were recorded, mounting brackets remain in place on the outsides of the exterior beams at four locations each in spans 2 and 6 (see Figure 3.3), and this type of measurement can readily be performed in the future.

3.4 Strain Measurements

The experimental setup had an extensive network of strain gauges, including both internal and external concrete strain gauges at various locations in Spans 2 and 6 of the bridge, which were oriented both laterally and longitudinally with respect to the bridge, and a few strain gauges on FRP bars in those spans. The general idea was to compare the relative stiffnesses of the FRP- and ECS-reinforced bridge decks under calibrated live loads. Live load tests within two years of the completion of the bridge would also set a benchmark for future live load tests.

The strain gauges installed on FRP bars were applied next to internal concrete strain gauges in an attempt to monitor differences in strain between the bars and the surrounding concrete. A significant difference of this type would indicate a lack of bond and composite action, that is, that forces were not being effectively transferred from the concrete to the FRP bar.

3.4.1 Strain Gauge Types and Locations

As indicated above, strain gauges were installed at multiple locations on the bridge in both longitudinal and transverse directions. Embedded concrete strain gauges were placed at the level of, and attached to, the top mat reinforcement and over the tops of the beams between the precast panels. Surface mounted strain gauges were placed on the tops of some precast panels (making them "internal" also in the sense that they ended up at midheight of the completed 8-inch-thick concrete slab) and on the bottom surfaces of the panels and beams. Also, two special embedded concrete gauges were placed at several overhang locations, and a few gauges were placed directly onto FRP bars.

Figure 3.4 shows longitudinally and laterally oriented embedded concrete strain gauges attached to ECS bars in the top mat of reinforcement over an exterior beam as well as one longitudinal gauge at the level of the bottom mat of reinforcement. Figure 3.5 shows where longitudinal and transverse surface gauges have been installed on the bottom of a precast panel and protected and waterproofed with pieces of neoprene. Finally, Figure 3.6 shows how pressure was applied during curing of a surface gauge mounted on the bottom of one of the beams.

Figure 3.4. Embedded Concrete Strain Gauges Over an Interior Beam

Figure 3.5 Surface Strain Gauges Centered on the Bottom of a Precast Concrete Panel

Figure 3.6 Jack System for Installing a Surface Strain Gauge on the Bottom of a Beam

The locations of the embedded and surface-mounted concrete strain gauges are shown in Figures 3.7 and 3.8, respectively. These figures are for the FRP-reinforced Span 6; mirror image figures would apply for the ECS-reinforced Span 2. In many places both longitudinal and lateral gauges were positioned together, as illustrated in Figure 3.5.

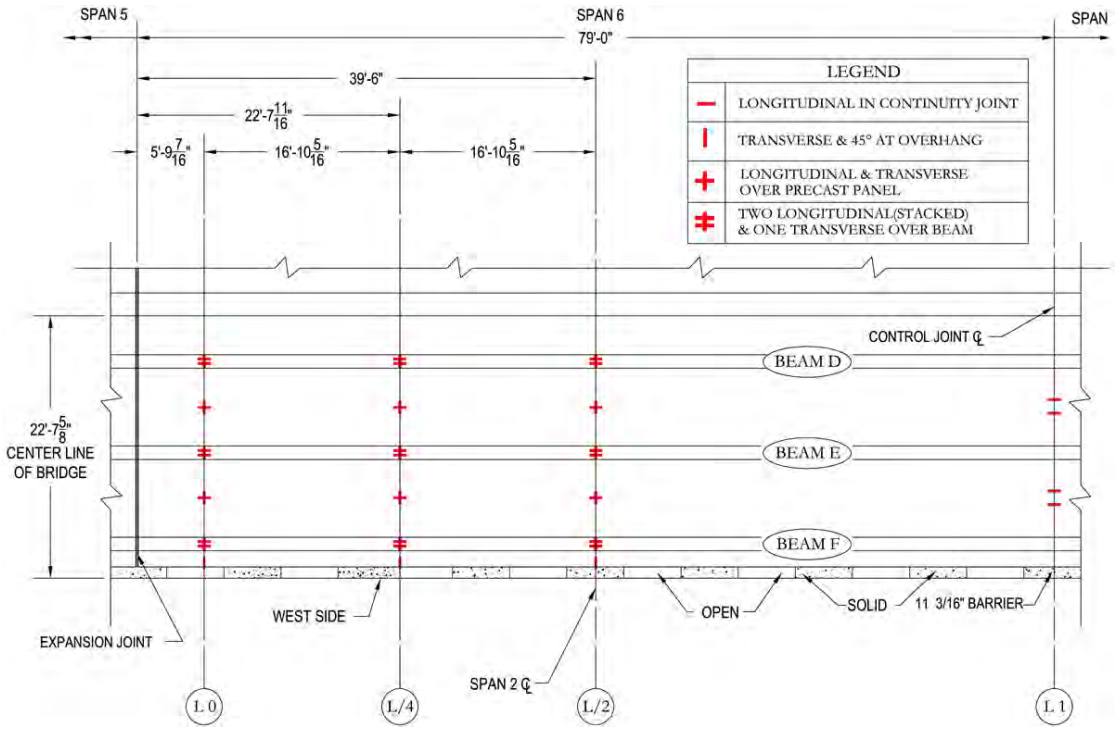

Figure 3.7 Embedded Strain Gauge Locations in Span 6

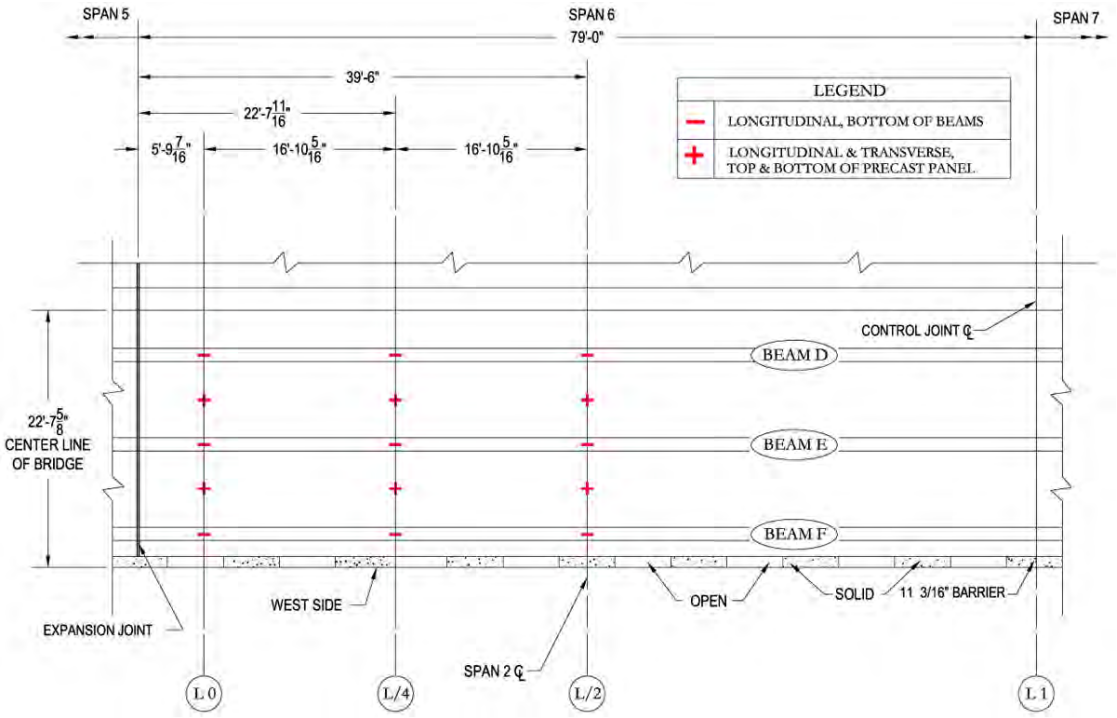

Figure 3.8 Surface-Mounted Strain Gauge Locations in Span 6

The special overhang embedded gauges are illustrated in Figure 3.9. The purpose of these gauges, which were installed at three locations in each of the instrumented spans, was to measure flexural tension and shearing strains at key points in the overhang. One gauge was positioned horizontally in the top mat of the reinforcement over the outside edge of the top flange of the supporting concrete beam. It was oriented in the transverse direction so that it would capture strains due to negative bending of the deck from a load placed on the overhang. The other gauge was located at the critical section for shear, that is, at mid-depth of the slab four inches outside the top flange of the concrete beam. It was positioned at a 45^{o} angle.

Figure 3.9 Embedded Strain Gauges at the Overhang of the Bridge Deck

Among the other strain gauges were gauges in the controlled joints between Spans 1 and 2 and Spans 6 and 7. Strains at these locations were of interest to researchers in regard to the hinging designed to occur there. Each of these joints was constructed with a fully cast-in-place concrete section approximately eight inches thick. Each had ECS rebar in the bottom mat and either ECS reinforcement or FRP reinforcement in the top mat, depending on whether the joint was between Spans 1 and 2 or between Spans 6 and 7. At the center of each controlled joint a chamfer was placed on the bottom surface and a plastic "zip strip" was installed in the top surface. These elements force the inevitable transverse crack at the joint to

follow a straight line and to form through the depth of the cast-in-place section. This method of construction has the effect of allowing considerable hinging between the two adjacent spans.

Embedded strain gauges placed at a controlled joint location are illustrated in Figure 3.10. These gauges were centered over the plane between the zip strip and the chamfer. This strategy was intended to allow the gauges to span across a crack in the concrete, secured to either an FRP or an ECS top mat bar. These gauges were placed to allow a direct comparison of the strains in the respective bars at these locations when wheel loads are placed on the adjacent spans.

Figure 3.10 Embedded Gauges in the Controlled Joint Between Spans 1 and 2

In order to use strain gauges to possibly monitor the bond between some FRP bars and the surrounding concrete, ¼-inch-long surface mounted gauges were installed on three different FRP bars. The bars were then installed in the bridge deck as a part of the top mat of reinforcement at three different locations. An embedded concrete strain gauge was then installed adjacent to each instrumented FRP bar. As previously discussed, any difference in strain between the gauges mounted on the FRP bars and the corresponding embedded concrete gauges could indicate a loss of bond between the FRP bars and the concrete.

3.4.2 Strain Gauge Specifications and Installation

The three different types of strain gauges used are designated in this section. First, the embedded gauges were Vishay 350-Ω concrete gauges as illustrated in Figures 3.4, 3.9, and 3.10. These gauges were four inches long and encased in a protective plastic sheath, which had a dimpled surface for increased bond to the surrounding concrete. Researchers installed these embedded gauges by using cable ties to secure the gauges to the top or bottom mat of the reinforcement as shown in the various figures. The gauge at a 45-degree angle in Figure

3.9 was tied to a 6-inch-diameter plastic spacer ring and this ring was then secured to the top mat reinforcement. It should be noted, however, that these rings were susceptible to being stepped on during construction by the workers, so the final positions of the 45-degree-angle gauges could not be ensured.

Second, the surface-mounted concrete strain gauges were all Micro-Measurements foil-backed, 120-Ω gauges. They had a two-inch gauge length. This length was selected to ensure that the gauges would encompass more than one piece of aggregate in the concrete and thus better represent the strain occurring in the concrete material as a whole at each location. In installing the surface mounted gauges, the concrete surface was first ground down with a masonry grinder so that the aggregate was exposed and the surface was smooth. The ground surface was then conditioned using Micro-Measurements conditioners A and B. Once the surface was conditioned and allowed to dry, Micro-Measurements epoxy resin was applied in a thin layer. The purpose of this thin layer was to fill any surface depressions, pores, and other irregularities. This epoxy coat was then allowed to cure a minimum of 6 hours (usually overnight). Once the layer had been sufficiently cured, it was sanded down to the level of the concrete surface using 200-gauge sandpaper. The surface was then cleaned and conditioned again using conditioners A and B and the surface mounted gauge was epoxied on. Once the gauge and its epoxy had been applied, pressure was maintained on the gauge for 6-8 hours as the epoxy cured. For the top surface locations (on the precast panels) this pressure was accomplished by placing a protective piece of plywood over the strain gauge and then placing a concrete masonry unit on top of the plywood. At strain gauge locations on the bottom surfaces of precast panels and beams, a frame was constructed of two by fours and plywood to hold a pneumatic jack against the strain gauge. This system can be seen in Figure 3.6.

Finally, the small strain gauges placed on three FRP bars were one-quarter-inch Micro-Measurements foil-backed gauges. The installation of these gauges provided quite a challenge to the researchers. Their installation could not utilize the method specified by Micro-Measurements for installation on concrete surfaces because grinding the surface of an FRP bar smooth would damage the fibers at that location, resulting in a loss of capacity in the bar. Furthermore, the strain gauges could not be applied directly to the surfaces of the bars because of the rough sand treatment on the surfaces. Therefore, researchers developed a special method for installing three strain gauges on the surfaces of FRP bars. First, duct tape was used to form a small square area on the FRP surface that would be filled using Micro-Measurements epoxy resin. This template was approximately ¼ inch by ¼ inch in plan and approximately 1/8 inch deep. Epoxy was then used to fill the square created by the template, also filling in the rough surface of the FRP bar. The epoxy was allowed to cure 6-8 hours, and then it was sanded and conditioned using Micro-Measurements conditioners “A” and “B.” Finally, the strain gauge was epoxied to the bar and pressure was applied using a screw-clamp.

3.4.3. Operable Strain Gauges

As mentioned earlier, some of the strain gauges installed in Spans 2 and 6 of the Phase II construction were found to be inoperable during the live load tests of December, 2001. Some of the inoperable gauges were damaged by construction workers, some had their lead wire

labels pulled off when the wires were passed underneath the bridge to the junction boxes, and others had their lead wires damaged by vandals. The vandal damage was visually evident before the tests, but there was insufficient time to install new wiring for all of the gauges with damaged wires for their inclusion in the tests. A special trip has since been made to test the remaining lead wires of all the stain gauges, and it was found that 69 of the 84 original gauges are still operable and have a known location in Span 6, while only 14 of the original 88 are still operable and have a known location in Span 2. The great majority of gauges in Span 2 had their lead wire labels pulled off, either in passing the wires to the junction box or by vandals. Appendix D gives drawings defining exactly which strain gauges are still operable.

The strain gauge data obtained in the live load tests of December, 2001, were quite voluminous, with measurements attempted from approximately 86 gauges during 24 different tests. These data are all available in Appendix B of the Master of Science Thesis of Jacob Bice (Bice, 2002). Only key strain data related to the stiffness of the top mat FRP reinforcement are presented and discussed in Chapter 4.

3.5 Corrosion Measurements

While corrosion measurements were not expected to be conducted during the term of this research contract, certain provisions were made to perform such measurements in the future after enough time has passed to possibly have rebar corrosion develop. In particular, three black steel reinforcing bars were installed in Spans 2 and 6 of Phase I to act as "corrosion bars." These black steel bars were equipped with wires extending outside the slab so that corrosion probability and rate measurements could be made at their locations. Obviously, such bars would represent the behavior of non-epoxy-covered steel reinforcing bars, which would provide a baseline of comparison with the behavior of both FRP and ECS bars throughout the bridge. The twenty-foot-long "corrosion bars" were placed transversely across the deck at three locations in each span and were bent up at the overhangs as starter bars for the barriers. Extending them into the barriers may allow measurement of their corrosion in the joint between the slab and the barrier, which is a particularly sensitive region. Figure 3.11 shows the locations of the corrosion bars in Span 6, Figure 3.12 shows the bar near the controlled joint (continuous end) of that span, and Figure 3.13 shows the bar near the sealed expansion joint (discontinuous end) of that span.

The corrosion bars have yet to be tested with corrosion measuring equipment, but they should be fully operational at such time as measurements are desired.

3.6 Crack Measurements

The use of FRP bars in concrete bridge decks is intended to improve the durability of the decks by avoiding corrosion of the steel reinforcing bars normally used. Such corrosion is made possible by cracking in the top surface of the deck. Top surface cracking, however, is affected by the stiffness of the reinforcing bars near the surface, and this stiffness is smaller for FRP bars than for steel bars. Other factors such as the ambient conditions at the time of casting and the presence of precast panels in some bays and not others can also affect deck cracking.

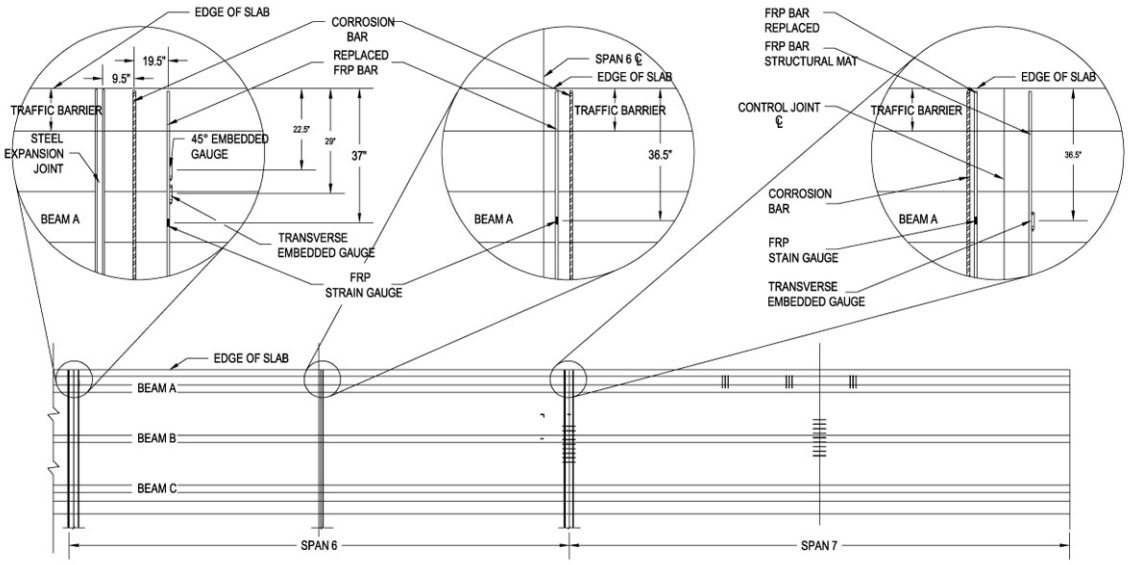

Figure 3.11 Locations of Corrosion Bars in Span 6 of Phase I

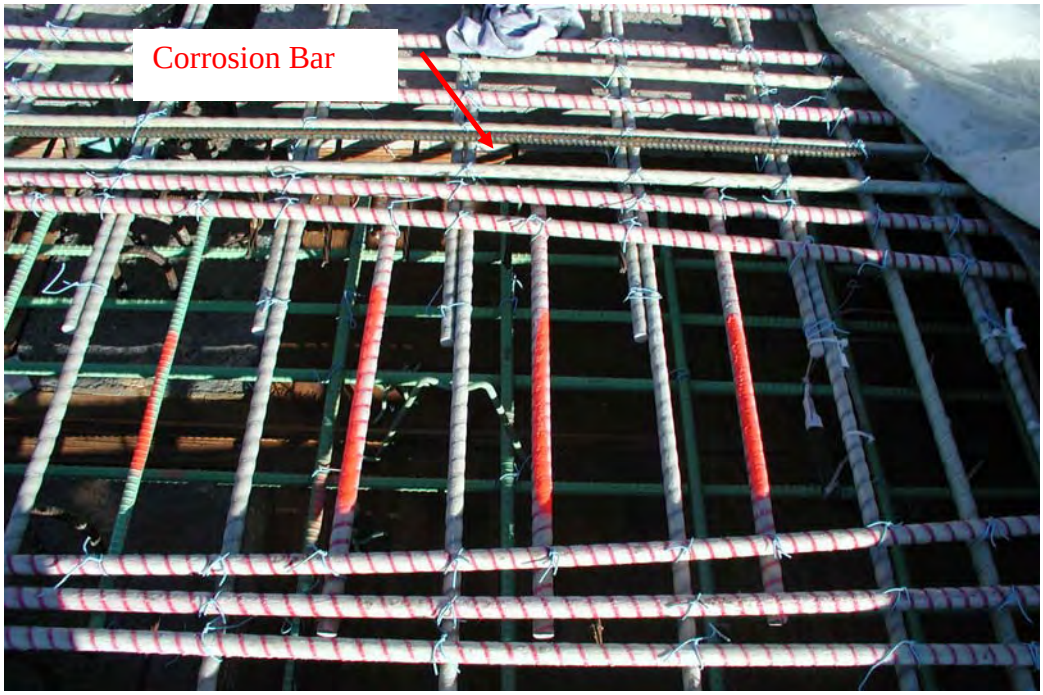

Figure 3.12 Corrosion Bar at the Controlled joint (Continuous End) of Span 6, Phase I

Figure 3.13 Corrosion Bar at the Sealed Expansion Joint (Discontinuous End) of Span 6, Phase I

In some cases deck cracking can lead to deterioration of the deck even without causing reinforcing bar corrosion.

In order to evaluate the influence of top mat FRP bars versus ECS bars in regard to deck cracking, a plan was devised to map the visible deck cracks in Spans 2 and 6 of Phase II. The cracks were expected to be mapped both with no load applied and with calibrated truck loads at various positions. In order to provide a systematic basis for this mapping, the segments of the deck in each span were labeled as shown in Figure 3.14. This figure is for Span 6 (and part of Span 7); a mirror image figure was used for Spans 1 and 2. The crack measurements are discussed in Section 4.4.

3.7 Witness Bars and Other Long-Term Performance Measurements

While cracking of the deck can be monitored over the long term as a performance measurement, other possible signs of deterioration should also be checked. These signs could include such problems as leaking of water where water should not penetrate or spalling of concrete at any location under the deck. The main special provision for long-term performance monitoring of the Sierrita de la Cruz Creek bridge, however, was installation of so-called non-structural “witness bars” at three locations each in Spans 2 and 6. The three locations were in the overhang, at midspan, and in the controlled joints. At each location in each span a set of nine bars was placed (three sets of three).

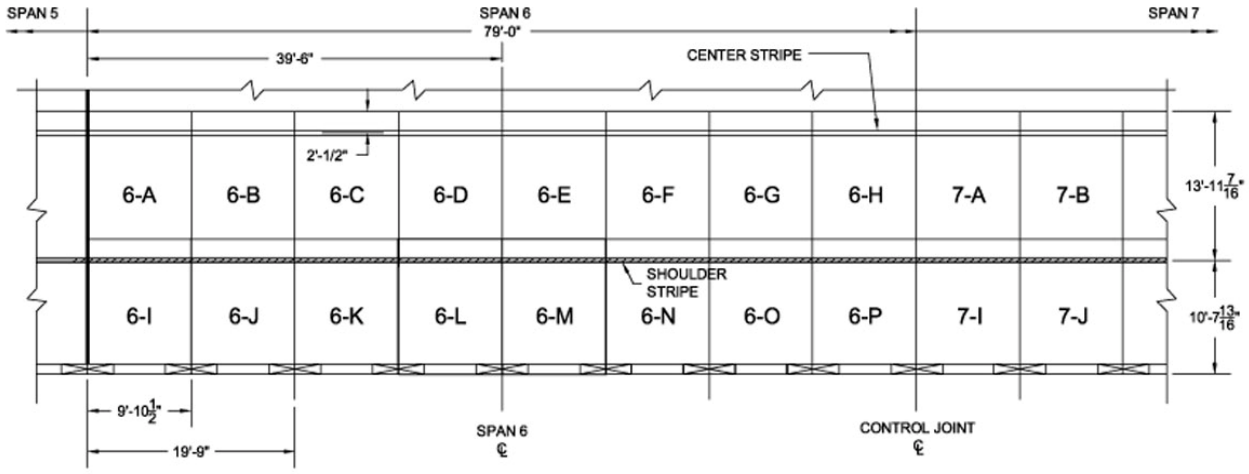

Figure 3.14 Labeling of the Deck in Spans 6 and 7 for Crack Mapping

The bars themselves were short (two-foot) segments of FRP, ECS, and black steel rebar to possibly be extracted from the deck at various later times for examination and testing of their condition. Figure 3.15 shows the locations in plan view of the bars for Span 6; mirror image locations were set up in Span 2. Figure 3.16 shows the set of FRP bars in place in the overhang of Span 2.

The concept behind installing the witness bars was to extract several sets of bars of the three different types in the FRP-reinforced span and in the ECS-reinforced span at different times in the future, say after three, ten, and thirty years. Examination of the bars would provide an indication of the on-going condition of the main FRP and ECS reinforcement in comparison to the condition of black steel reinforcement, had black steel been used. While the FRP witness bar lengths are not long enough to allow for standard tensile testing, the bars can be examined for water absorption, mass loss, chemical attack at their ends, and other potential problems.

It is recommended that, using the carefully documented dimensions to the witness bar locations as shown in Figure 3.15 and further documented in Appendices A and B, the witness bars be extracted by saw cutting into the deck at an angle from each side and from the ends and "popping" the resulting wedge-shaped segment out of the slab. The witness bars were spaced one bar diameter (3/8 inches) above the top mat reinforcement, but to insure that cutting out the witness bars would not weaken the slab by possible rupture of top mat bars, extra "reinforcing" bars were placed around the witness bar locations. These bars, shown at the left and right in Figure 3.16 and in plan in Figure 3.17, should provide the strength and stiffness lost by any accidental cutting of regular top mat bars.

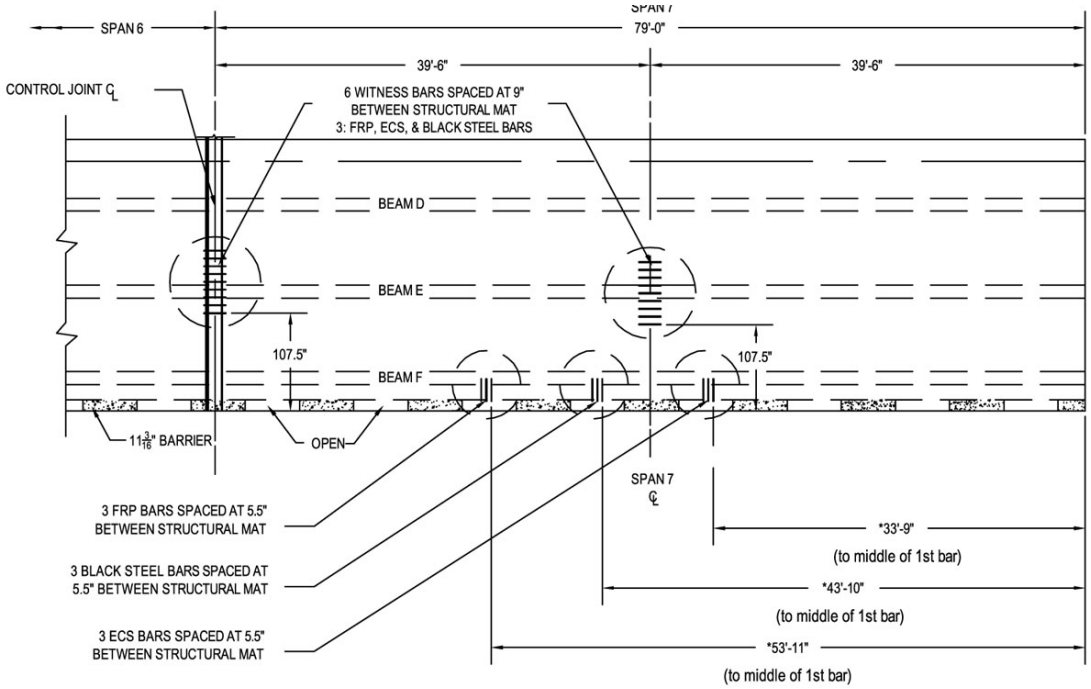

Figure 3.15 Witness Bar Locations in Span 7

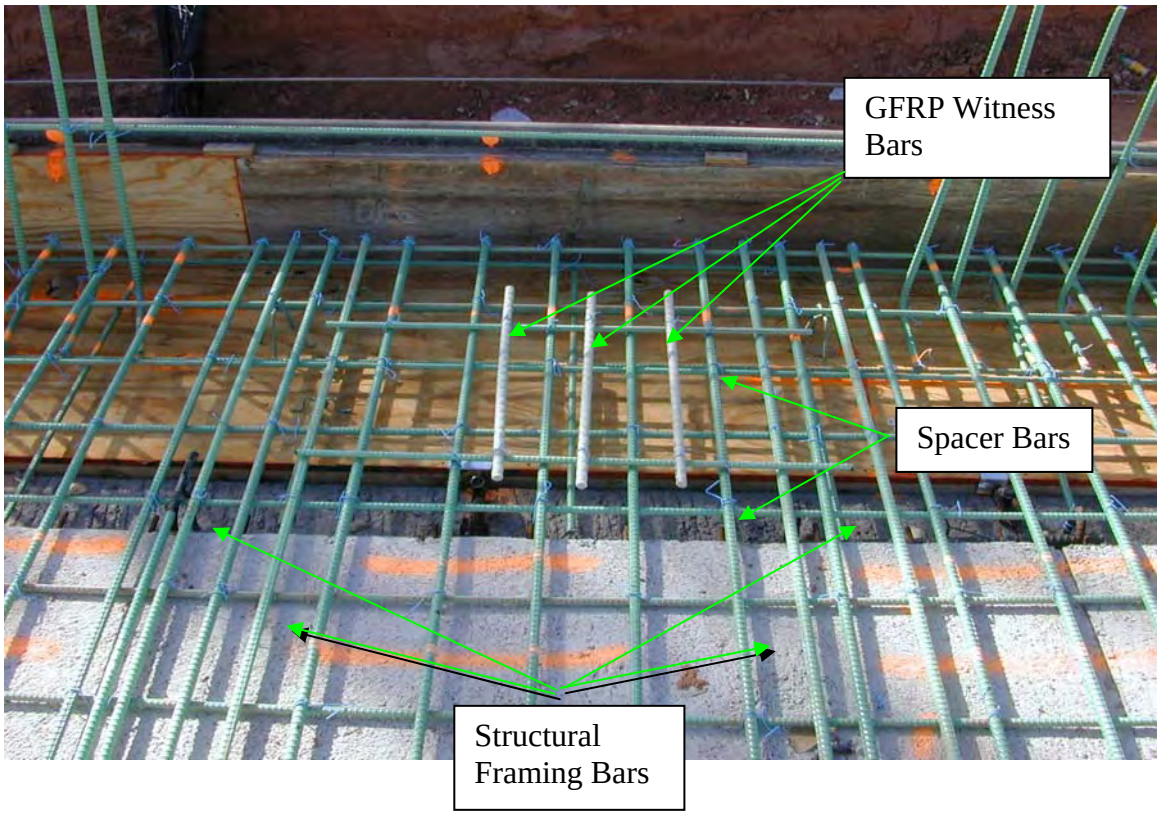

Figure 3.16 A Set of Three FRP Witness Bars in an Overhang

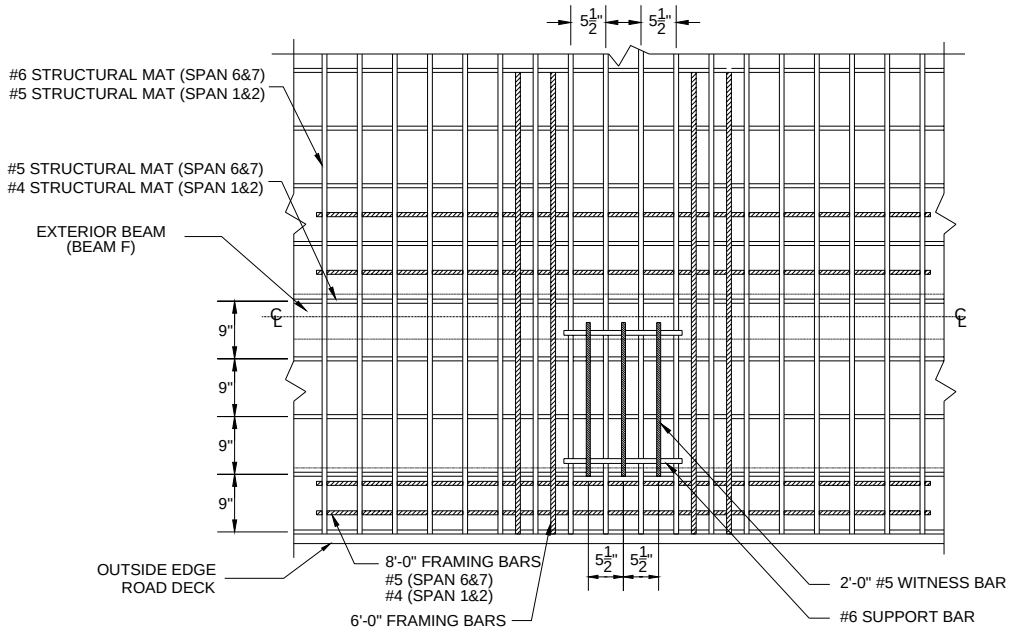

Figure 3.17 Detail of Transverse Witness Bars and Their Framing Bars in an Overhang

3.8 Data Acquisition System

The weather and temperature measurements at the site were recorded on a datalogger as described in Section 3.2, but data from both types of electronic live load test instruments (displacement transducers and strain gauges) were recorded by means of a portable desktop computer. For data acquisition (DAQ), LabView software, a graphical interface programming language by National Instruments, Inc, was utilized in conjunction with a National Instruments SCXI system. In order to record the 112 channels of strain gauge data, the SCXI system employed seven 16-channel SCXI 1122 modules combined with seven SCXI 1322 signal conditioning modules. For the eight LVDT measurements the SCXI system employed one eight-channel SCXI 1120 module with a SCXI 1320 signal conditioning module. All of these modules were mounted in one National Instruments 1001 chassis. An example of a SCXI data acquisition system is shown in Figure 3.18.

The 16-channel modules used with the strain gauges were well-suited for acquiring strain data. The default excitation voltage of the modules (3.333 V) was correct for the gauges, and the module gain, or signal amplification, could be boosted to a level required for the acquisition of small changes in voltage (typically ± 5 mV) from a fairly lengthy distance. Also, the signal sensing capability of the SCXI-1122 modules allowed the lead wire resistances to be neglected when determining the strains from such distances.

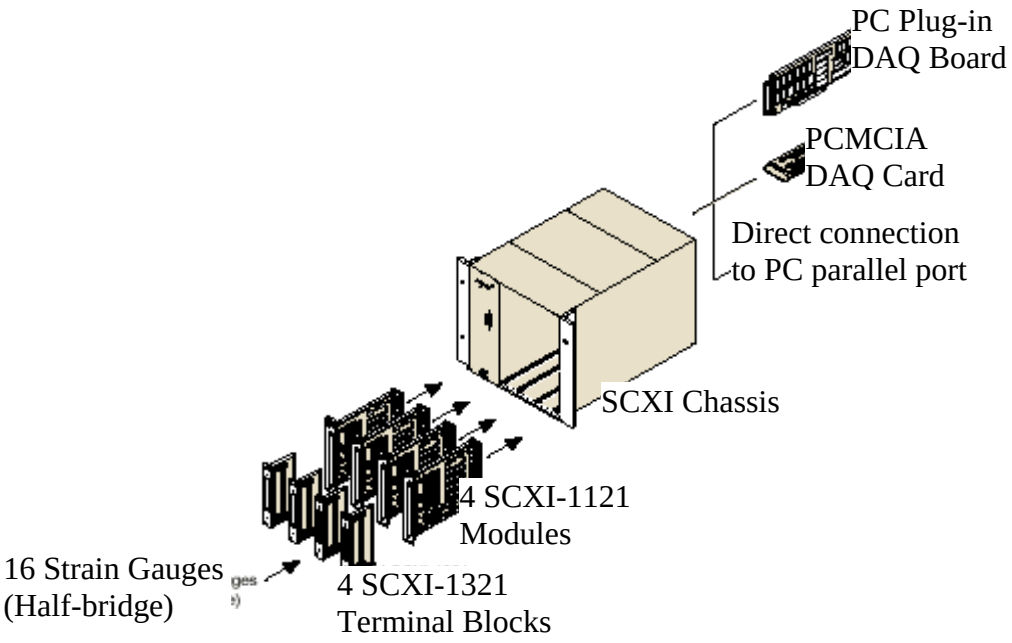

Figure 3.18 Example of a SCXI DAQ System (Source: National Instruments 2002)

The average lead wire length for this application was 60 ft. The SCXI system provided a current of 225 mA at 3.333 V, which could run the 16 120-Ω strain gauges in each module in a quarter bridge configuration. The "dummy" resistors required for the quarter bridge configuration were mounted on a barrier board. The long lead wires and the small changes in voltage required a gain of 1000. The 8-channel module used to acquire the deflection data was selected because the LVDTs used required a greater excitation than the strain gauges, 5 V compared to 3.333 V.

A program written in LabVIEW controlled the data acquisition hardware. The system ran in a multiplexed mode and sampled data from each channel in a module before moving to the next module. Although the computer system was capable of taking samples at a very rapid rate, switching of a common voltage source from one strain gauge channel to the next within a module took some time and required sampling of each strain channel a number of times until transient voltages died down. As a result, sampling all of the channels took, on average, 1.5 minutes. While this sampling rate was adequate for static load testing, it would not be adequate for dynamic testing.

During the first live load test performed on the Sierrita de la Cruz Creek bridge, the computer was set up under the bridge, along with the set of barrier boards to which the instrument lead wires were attached.

3.9 Instrumentation Utilization

As indicated earlier, some of the instrumentation set up for monitoring the performance of the Sierrita de la Cruz Creek bridge was intended only for long-term monitoring. Specifically, the black steel "corrosion bars" and the GFRP, ECS, and black steel "witness bars" will only

be utilized, if at all, at different times in the future. However, other portions of the instrumentation were implemented during and soon after the completion of the bridge. These studies included temperature measurements in the deck during and following the Phase II pour, deck surface cracking and deck strain measurements during one set of static live load tests, and deflection and crack development measurements during more abbreviated second live load tests. The results from this work are present in Chapter 4.

All of the long-term monitoring systems (corrosion bars and witness bars) remain operable for future testing. The weather station initially installed at the site has been dismantled, but, despite some damage, much of the remaining instrumentation is also available for future measurements. The greatest losses have been to the strain gauges, but as documented in Appendix D, 69 out of the 84 strain gauges in Span 6 remain operable and have a known location, while in Span 2 only 14 of the original 88 strain gauges are still operable and have a known location. The ten thermocouples in each of two deck panels are operable, and deck edge displacement measurements can be made with the aid of existing mounting brackets on the exterior beams. Of course, future crack measurements in the deck can also be made at any time.

CHAPTER 4. SHORT-TERM MEASUREMENTS

4.1 Introduction

The instrumentation designed for and installed on the Sierrita de la Cruz Creek Bridge was intended for the study of both long-term and short-term effects. As discussed in the previous chapter, virtually identical instrumentation was placed in and on two ECS-reinforced Spans (1 and 2) and the anti-symmetric FRP-reinforced Spans (6 and 7) for direct comparison. The anticipated long-term studies could include monitoring of the overall bridge condition, measuring and mapping the top surface cracks in the deck, performing corrosion tests on embedded black steel bars, removing the three types of "witness bars" from the deck and examining them, and carrying out live load tests from time to time. These long-term studies are beyond the scope of this research project and this report. Obviously, the shortest-term study has already been made and will not be repeated – the measurement of temperatures in the deck during and immediately after casting. The other short-term studies that have been completed were two tests of the bridge's cracking, deflection, and strain behavior under static live loads imposed by fully loaded TxDOT dump trucks. Such tests can be repeated in the future.

The deck pour for the first phase of the bridge construction took place on July 14, 2000, a very hot summer day. The deck pour for the second phase of the construction took place on November 16, 2000, a rather cold fall day. Temperature measurements are reported herein only for the latter event. The first set of live load tests was conducted on December 12 and 13, 2001, just over a year after the second phase deck pour and less than a year after the bridge was opened to traffic. The day was very cold and windy. The second live load testing took place on September 16, 2002, almost two years after the second phase deck pour and after the formal end of the research project. This chapter reports on the procedures used and the key findings obtained in November, 2000, December, 2001, and September, 2002. Specifically, the temperature measurements, crack mapping studies, and live load test results are presented.

4.2 Temperature Monitoring

The procedure for the temperature measurements taken during casting of the second phase Span 6 deck on November 16, 2000, was direct. The Campbell Scientific data logger was set to record the temperatures from the ten thermocouples installed around and over the one precast panel in Span 6 of the deck (see Figure 3.2). Readings were taken at 30-minute intervals. Recording began at midnight on the morning of the pour and extended through two weeks after the pour. The hours immediately after the pour reached the location of the instrumented precast panel provided the data of greatest interest.

Figure 4.1 shows the temperatures recorded within the second phase bridge deck for six days starting at midnight on the morning the second phase deck was poured, along with ambient temperatures. Figure 4.2, which shows the same results for the first two days (November 16

and 17) in more detail, is intended to indicate more clearly what happened before and immediately after the concrete pour reached the location of the thermocouples. The pour for that day began in Span 7 at 10:15 a.m. and reached the precast panel in Span 6 that was instrumented with thermocouples around 2:30 p.m. The pour was completed about 4:00 p.m.

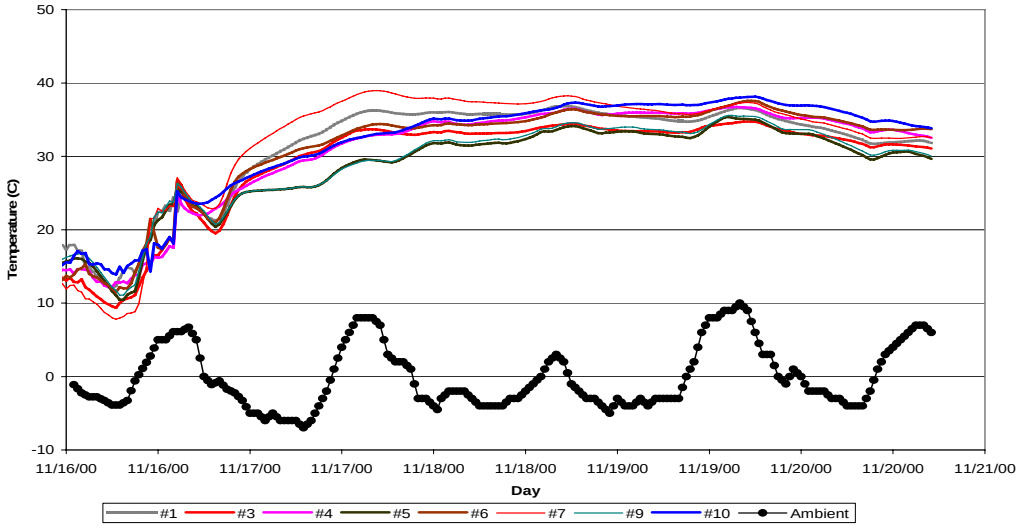

Figures 4.1 Thermocouple and Ambient Temperatures for Six Days Following Span 6 Pour, 2nd Phase

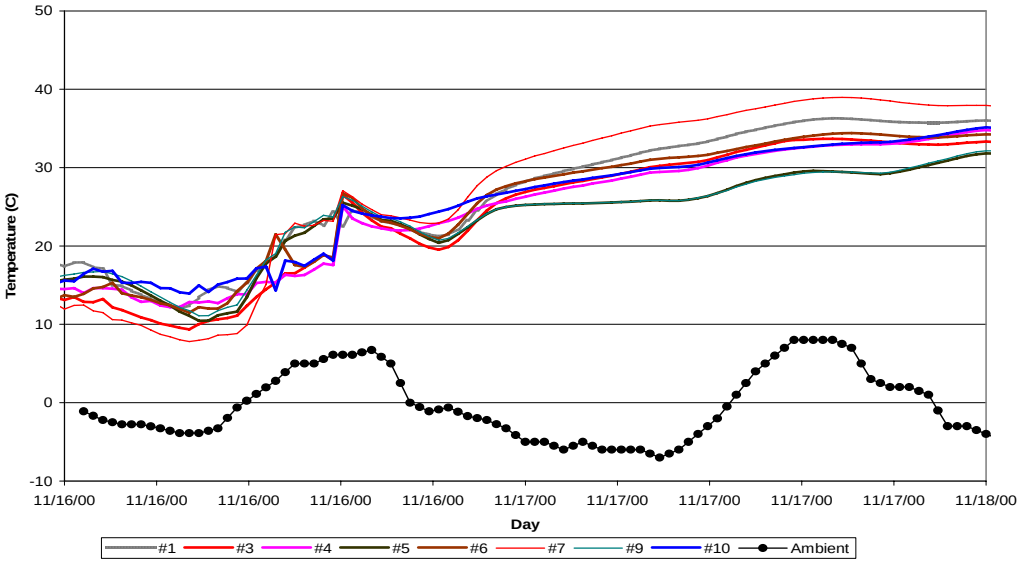

Figures 4.2 Thermocouple and Ambient Temperatures for Two Days Following Span 6 Pour, 2nd Phase

Figure 4.2 shows that on the day of the pour all of the thermocouples had low temperatures while exposed to the open air. There was a cool north wind, and just before the sun came out (about 7:00 a.m.) the thermocouple temperatures dropped to the range of 8-14^{o}C (46-57^{o}F) while the ambient temperature dropped to about -4^{o} C/25^{o}. Then during the morning and mid-

day hours, with the air temperature rising and the sun shining on the thermocouples, their measured temperatures rose to approximately 25°C (77°F) before they were engulfed by concrete about 2:30 p.m. Immediately after the concrete was poured over the thermocouples, their temperatures dropped due to the lack of sunlight and the cooling effect of the wet concrete. This cooling continued, along with cooling of the ambient air, until about 7:00 p.m., when there began a steady increase in the thermocouple temperatures primarily due to the heat of hydration of the concrete. Also, underneath heating was applied by the construction crew in view of the low ambient temperatures. The elevated thermocouple temperatures persisted for several days, as seen in Figure 4.1. The temperature tended to be greatest in the thermocouples closest to mid-depth in the combined slab (precast panels and cast-in-place portions), as these thermocouples were farthest from the surfaces that allowed conduction to the cooler surrounding air. The peak temperature in any thermocouple at any time was 39°C (102°F) at 4:00 p.m. on November 17. After that time the temperatures stayed rather steady for two days, with slight daily peaks around 4:00 p.m. each day, before gradually decreasing. This pattern of temperature rise and decay due to the hydration of the deck concrete was expected.

The main lesson to be gained from the temperature measurements in the deck during the second phase pour is that the peak temperatures did not quite reach the lower end of the temperature range at which Nishizaki and Meiarashi (2002) began to observe a reduction in tensile strength of GFRP bars 40°C (104°F). This held true despite the underneath heating that was applied. This heating was decided upon by the Regional Engineer because of the low ambient temperatures at the time of the pour. If the pour had been during a hot summer day, however, the peak temperatures in the concrete would have undoubtedly risen quite a bit higher.

4.3 Live Load Test Procedures

The procedures adopted for the live load tests on December 12 and 13, 2001, were fairly complex. Basically, the on-going traffic was stopped entirely during each set of measurements with either one or two fully loaded TxDOT dump trucks positioned at pre-planned locations on the west side (second construction phase) of the deck. Fourteen tests were performed on the FRP-reinforced Span 6 and ten of the same tests were performed on the ECS-reinforced Span 2. Between measurements, the traffic was alternately allowed to pass in single file on the east side (first phase) portion of the bridge. The dump trucks had been carefully weighed and each had a rear double-axle load of 29.4 kips and a front single-axle load of 24.6 kips. The traffic control and the testing were performed under the direction of TxDOT Amarillo Area Engineer Joe Chappell and researchers at Texas Tech.

The positions prescribed for the trucks were designed to maximize negative and positive moments in certain portions of the deck, particularly the negative lateral moments over the longitudinal supporting beams, the negative lateral moments in the overhangs, and the positive lateral and longitudinal moments between the beams. Deflection and strain gauge data were expected to correlate with these moments. Before the load tests researchers laid out the grid shown in Figure 3.14 for Spans 6 and 7 and a similar one for Spans 1 and 2. Then they recorded the cracks that had developed in the top surface of the deck in these spans under

zero load conditions. Later, during the load tests, the same type of crack mapping was performed with the trucks in their prescribed positions. Both the locations and the widths of the cracks were recorded.

Figure 4.3 shows the two dump trucks being positioned back-to-back in Span 6 with their outside wheels as far out on the overhang as possible. In this case the rear wheels were ridden up onto two transverse steel channel sections supported by 4x4-inch wooden blocks to cause the rear axle loads on the deck to be concentrated on smaller areas than the tire prints would have allowed. This technique was used throughout the Span 6 tests, but in the tests in Span 2 the channel sections were not used because it took extra time and it was not expected to affect the results significantly.

Figure 4.3 Crack Measuring with TxDOT Dump Trucks in a Back-to-back Load Case
Photograph: Courtesy of Alvin Gutierrez, FHWA

For each series of live load tests (first on Span 6 and then on Span 2) the zero values of the strains and displacements to be recorded were taken just once before the first loads were applied. Then, with the truck or trucks in place for each test, the computer swept over all of the data channels, subtracted the zero values, and stored the results in a file. As mentioned earlier, vandalism that resulted in many lead wires being destroyed and a malfunction of the

displacement module and one strain gauge module significantly diminished the quality of the data recorded by the computer. However, manual total station deflection readings were taken and the cracks in the deck surface were mapped both before and during the loadings.

4.4 Cracking Results

As indicated in Section 3.6, cracking in the top surface of the deck of the second phase portion of the Sierrita de la Cruz Creek Bridge was measured and mapped in Span 2 (with ECS reinforcement) and in Span 6 (with GFRP reinforcement) on December 12 and 13, 2001. These measurements were made approximately 11 months after this part of the bridge was poured. The mapping, which utilized the segment layout of Figure 3.14, was first carried out with no load on the deck. Then the surface near the truck or trucks was carefully examined for new cracks during each of the live load cases, and the pre-existing cracks were measured for possible increases in length or width.

The general result was that a number of cracks were observed under no load, but when loads were applied to the bridge deck no new cracks formed in either of the spans tested. This behavior held true for all of the numerous loading conditions. Also, none of the existing cracks measurably propagated in length or increased in width under load. This result implies that all of the measurable cracks in the first year were either shrinkage, temperature, or reflective type cracks. It will be interesting to see if similar trends continue over the lifespan of the bridge.

Examination of Figures 4.4 and 4.5, which show the overall crack patterns of the two spans, reveals that the patterns were very similar. There was one noteworthy difference, however, in that there was a distinct longitudinal crack in Figure 4.4 for the GFRP-reinforced span that did not appear in Figure 4.5 for the ECS-reinforced span. This longitudinal crack was over the third beam from the west edge of the bridge, the beam adjacent to the full-width, cast-in-place bay of the bridge.

There could be several reasons for the formation of this longitudinal crack in Span 6 but not in Span 2. First, the mixes used at the two locations could have differed enough to influence the behavior. Second, the ambient temperatures at the different times of placement could have had an effect, as Span 2 was poured six days later than Span 6 (November 22 as compared to November 16), and the ambient temperatures were consistently five degrees Celsius (9^{o}F) higher on Nov. 22 than on Nov. 16. Third, other construction differences, such as flaws in the placement of the cast-in-place concrete or the application of underneath heating in Span 6 but not in Span 2, could also have contributed to the difference in cracking. Heating was not attempted in Span 2 because it was so much higher above the ground. Fourth, it is possible that prior to cracking the bond between the FRP reinforcement and the concrete was not fully developed and some slipping occurred. Researchers observed that the embedded sand surface treatment on the FRP bars tended to wear away as construction workers walked over the FRP mat. The worn surface treatment could possibly have reduced the bond between some of the FRP bars and the concrete. Finally, there is also the possibility that the greater stiffness of the epoxy-coated steel in the top of the deck in Span 2 influenced the lack of formation of a longitudinal crack there as compared to the more flexible GFRP reinforcement in the top of

the deck in Span 6. As shown in Table 1.1, the equivalent axial stiffness of the GFRP bars in the transverse direction (perpendicular to the observed longitudinal crack) was slightly less than half that of the steel.

In considering all of these factors one should keep in mind that since the unique longitudinal crack failed to open further under the loads that were applied in December, 2001, it appeared that the crack was not load-induced but caused by shrinkage and/or temperature effects.

Unfortunately, the unique longitudinal crack in the FRP-reinforced slab (and the absence of a similar crack in the steel-reinforced slab) was not fully recognized until all data sheets were thoroughly analyzed upon completion of the live load tests of December, 2001. Researchers therefore returned to the bridge in September of 2002 and placed loads specifically intended to widen the longitudinal crack found in Span 6. Two trucks were positioned over the crack in order to cause a critical loading. The locations of these two trucks are shown in Figure 4.6. This loading also failed to propagate the crack. However, unloaded crack widths taken on that day ranged from 0.01 mm to 0.02 mm versus the 0.01-mm to 0.013-mm widths measured in December, 2001. While crack width measurement using a comparison card is somewhat subjective, these results may indicate some widening of the longitudinal crack over the nine months following the initial crack mapping. Therefore, long-term monitoring of this crack should be of interest.

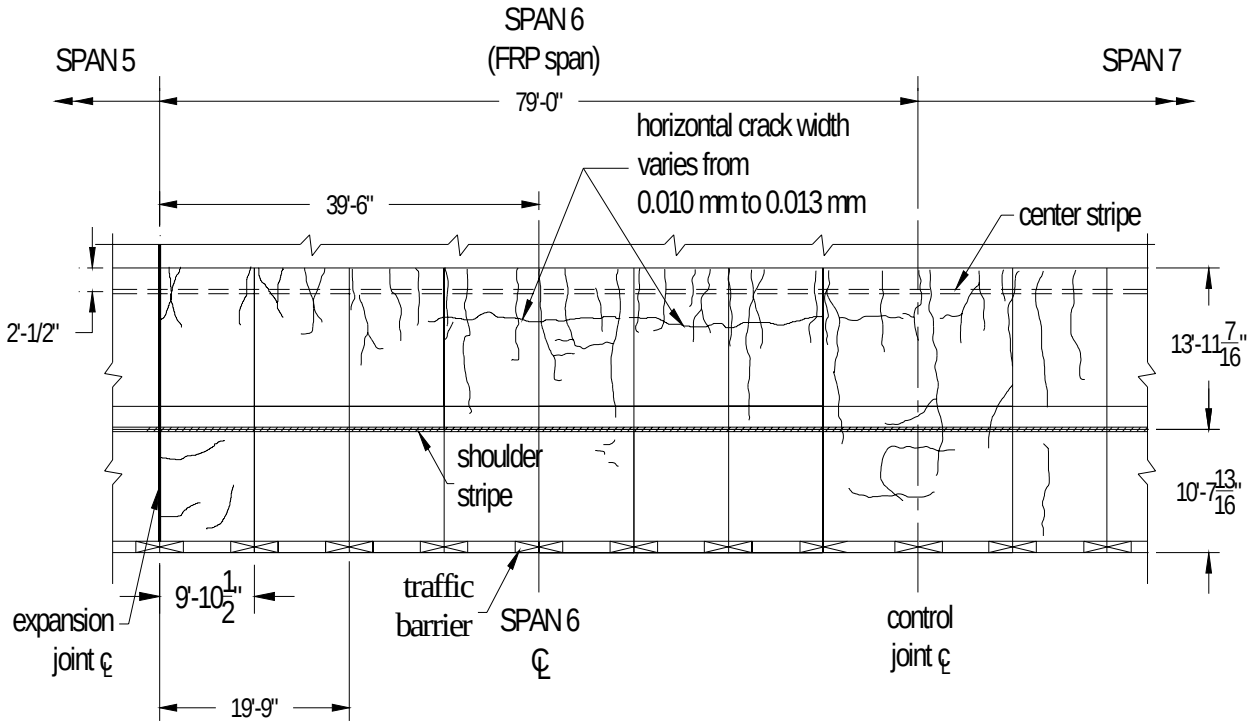

Figure 4.4 Cracking After One Year of Service in Span 6, Reinforced with GFRP

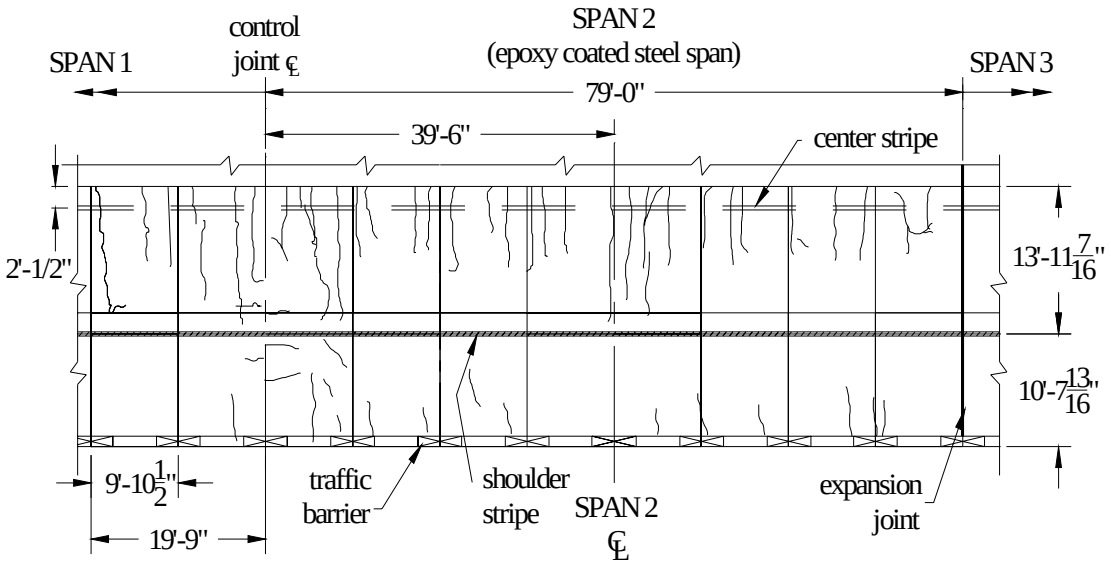

Figure 4.5 Cracking After One Year of Service in Span 2, Reinforced with ECS

Future efforts to monitor the longitudinal crack that formed in the FRP-reinforced span should be made not only to observe any propagation of the crack that might occur but also to classify the crack as either temperature or shrinkage induced. Determining the nature of this crack could provide answers as to why it formed in one span but not in the other. Monitoring the crack widths at specific locations during both hot and cold seasons could help to define the crack as a temperature crack. Finally, if a finite element model of the bridge were developed it could determine the stresses that might occur in the area of the crack due to temperature variations and perhaps predict whether or not a crack might be expected to form in this location due to these variations.

4.5 Displacement Results

As presented in Section 3.3, LVDT's were designed to be mounted on the sides of the exterior bridge beams in such a way that relative deflections between the edges of the deck and these beams could be measured at several points during live load testing. For the second phase part of the FRP-reinforced Span 6, this type of measuring system was designed bordering Piers 6 and 7 and at midspan. A similar arrangement was installed in the ECS-reinforced Span 2. However, during the main series load tests conducted in December of 2001 there was a malfunction in the data acquisition system module assigned to the LVDT's and no useful results were obtained. This was later attributed to a software programming problem related to the conditioning of the LVDT signals. While the program appeared to process LVDT data properly during debugging runs in the laboratory, it did not do so in the field.

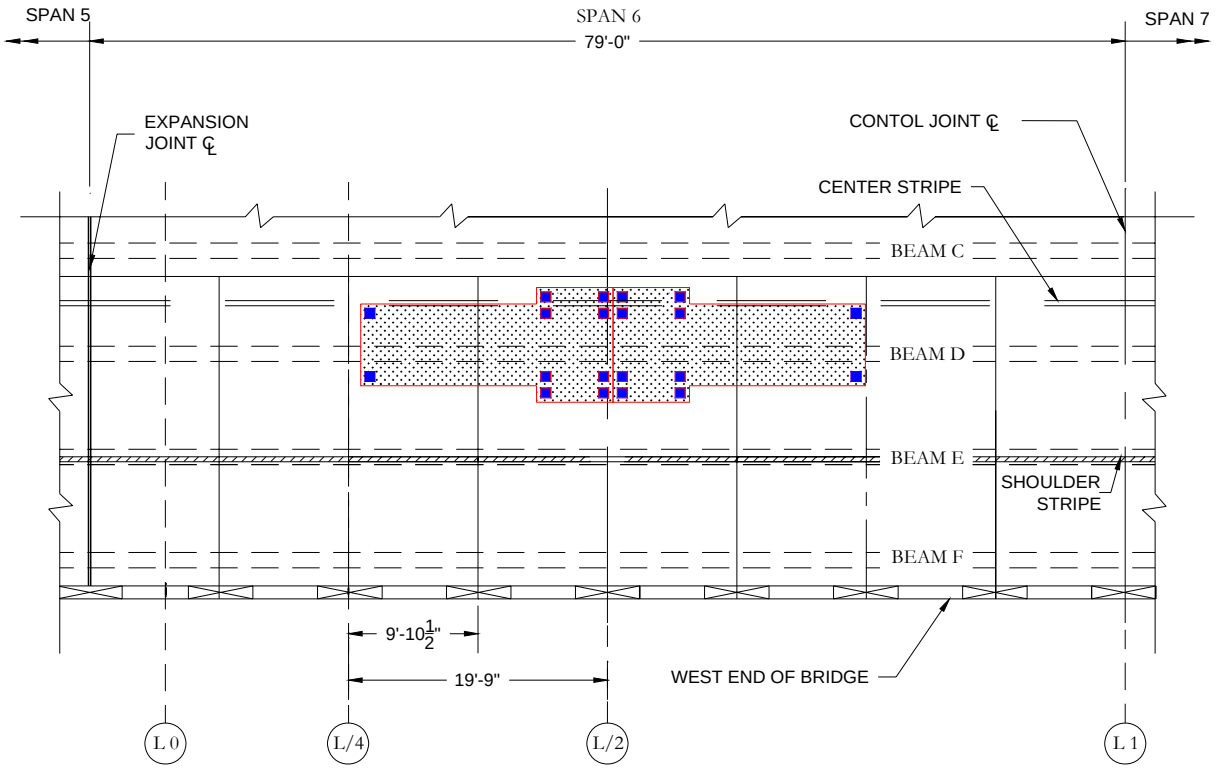

Figure 4.6 Truck Positions for Supplemental Crack Testing

A different type of deflection measurement was made during the supplemental load testing conducted in September of 2002. While the main objective of this testing was to determine if the longitudinal crack in Span 6 was load-induced, as discussed in the previous section, a total station was employed to measure the vertical displacements of the center points of Spans 6 and 2 with one and two 43-kip trucks parked near midspan. Figure 4.7 shows the positions of the trucks with two of them stationed side-by-side in Span 6.

The trucks could not be placed any closer to midspan and still allow the surveyor's rod to be positioned on the bridge centerline at midspan, as indicated in the figure. The metric side of the surveyor's rod, shown in Figure 4.8, was read, and the smallest division represented a height of 2 millimeters (0.08 inches). Thus, the accuracy of the readings was only about 1 millimeter (0.04 inches), and the loading that was applied only induced deflections of the order of 1.5 to 3 millimeters (0.06 to 0.12 inches), so only very approximate comparisons between cases could be made. Table 4.1 shows the values recorded with one truck and with two trucks on both Span 6 and Span 2.

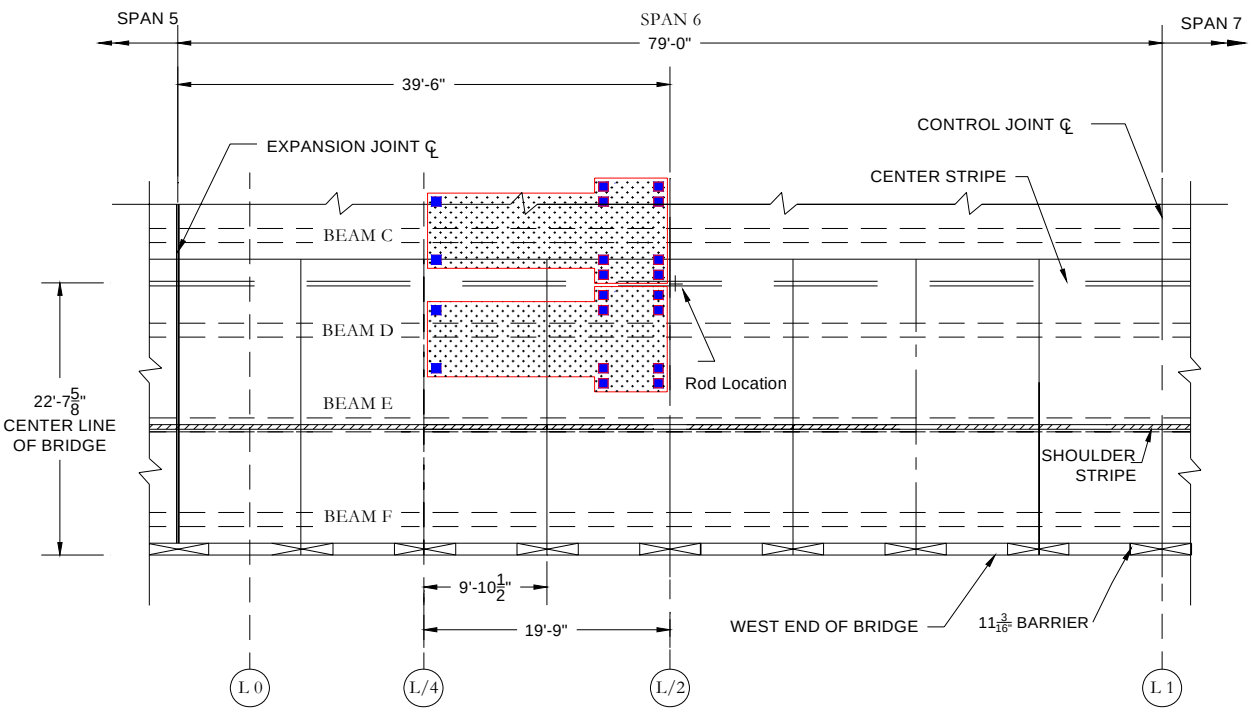

Figure 4.7 Truck Locations for Deflection Measurement of September, 2002

Table 4.1 Center Point Deflections Under Live Loading

Type of Value	FRP-reinforced Span 6		ESC-reinforced Span 2	
	1 Truck	2 Trucks	1 Truck	2 Trucks
Measured (mm)	1.50	2.00	2.00	3.00
Calculated (mm)	2.14	4.29	2.14	4.29

Several factors need to be considered in interpreting these data. First of all, the measured deflections were due mainly to overall longitudinal flexure of the composite beam-slab system, and the different types of top mat reinforcement (FRP and ECS in the two spans), acting in compression during this behavior, could hardly have made much difference. The slightly larger deflections in the ECS-reinforced span would, in fact, be opposite to the trend to be expected if the slab reinforcement did make a difference.

The differences in measured deflection between the spans, if not due to a lack of precision, could more easily be due to other differences. One possibility is a difference in slab thickness as the contractor had to grade the top of the slab for ride quality and had the leeway to make the slab thicker or thinner in different parts of the bridge to provide the proper grade.

Figure 4.8 Surveyor's Rod Used for Deflection Measurements of September, 2002

It was observed by the researchers through the use of probes that in a number of places the top of the slab was above the top mat reinforcement by an amount greater than in the design. Also, the deflection differences could have been affected by the supporting beams having different elastic moduli as a result of their manufacturing process. These beams were the main components providing flexural stiffness during the deflection tests, and differences in mix characteristics, curing conditions, etc., are capable of producing modulus differences.

An estimate of the center point deflection to be expected can be calculated by considering the entire composite bridge system to be a simply supported beam over its span length of 79 feet. The moment of inertia of the six-beam section, neglecting the barriers and the slab reinforcement, was calculated to be approximately 1.91×10^6 in^4 with the slab assumed to be a uniform 8 inches thick. Taking both the beam and slab concrete to have normal weight and a cylinder strength of 6,000 psi, the modulus of elasticity for the composite section was 4.415×10^6 psi. Then the calculated center point deflections, taking the front axle of each truck to carry 12.3 kips and each of the two rear axles to carry 14.7 kips (as measured by TxDOT) at the positions along the length shown in Figure 4.7, were 2.27 mm with one truck and 4.54 mm with two trucks for either span, as shown in Table 4.1. Both of these calculated values are larger than the measured deflections for the FRP-reinforced and ECS-reinforced spans. The assumption of a simply supported span could account for part of the difference; the controlled joint slab over the pier at one end of the span can provide a small amount of rotational stiffness because the slab is reinforced and the elastomeric pad supports exert a

restraint during rotation due to their stiffness. Other factors could be the additional moment of inertia contributed by the railings and the possibility that the slab thickness was greater than the design value of 8 inches.

One other factor in the measured deflections relates to the fact that the two-truck measurement was less than twice the one-truck measurement in each span. This lack of linearity suggests that in placing the trucks side-by-side as shown in Figure 4.7, more of the central beams were engaged and the overall longitudinal flexural stiffness of the system was greater in resisting the larger loads. This behavior indicates that considering the entire width of the bridge was not appropriate in the calculations above. Instead, lateral dishing toward the center of the bridge occurred both with one truck and with two trucks, and the outside beams were not fully effective. This lateral effect is difficult to account for without a three-dimensional model of the bridge. The fact that such dishing would tend to make the calculated deflections larger than the values determined above, and thus even more in disagreement with the measured deflections, suggests that the true longitudinal stiffness was underestimated.

4.6 Strain Gauge Results

Installing the extensive array of strain gauges depicted in Figures 3.7 and 3.8 proved to be both a benefit and a problem for this research effort. On the one hand, having so many gauges meant that even after some were damaged quite a few were left to provide data. On the other hand, the large number of gauges complicated the measurement setup in the field and the operation of shifting the computer and re-establishing all of the connections from Span 6 to Span 2 at the midway stage of the tests. It was expected during the December 2001 live load testing that the strain gauges would give the most significant results, but that expectation was compromised by vandalism, accidental damage to the gauges by the construction workers, and a malfunction in one of the seven data acquisition modules employed by the computer to take strain data.

In light of these developments, the presentation in this chapter includes an overview of the full set of live load tests, but actual results are given for only one representative load case.

4.6.1 Live Load Cases Considered

The test plan for the live load tests included 12 cases, symmetric about the mid-length of the bridge, for each end of the bridge. These cases for the ECS-reinforced end (Spans 1 and 2) are described briefly in Table 4.2 and illustrated by individual drawings in Appendix C. Two tests were actually carried out with the same set-up, but with the trucks slightly closer to the railing, for two of the cases listed in Table 4.2. As an example illustration, Figure 4.9 shows the position of the one truck used for Load Case D when considered for Span 6. By having the truck straddle Beam E a transverse negative moment was induced over this beam, causing the top mat reinforcement to undergo tension. One purpose of this test was to see if this negative moment would induce a longitudinal crack or widen an existing one over that beam. Another purpose was to measure the magnitudes of the strains in the vicinity, especially the lateral strains at the top mat level.

Table 4.2 Live Load Test Cases of December, 2001

Letter Desig-nation	No. of Trucks	Loaded Span(s)	Longitudinal Position(s) - of Rear Wheels if Only One Truck	Lateral Positions(s)
A	1	1	At midspan	Over centerline
B	1	2	At midspan	Over centerline
C	1	2	At midspan	Centered over 1st int. beam E
D	1	2	At L/4 from expansion joint	Centered over 1st int. beam E
E	1	2	5'-9.5" from expansion joint	Centered over 1st int. beam E
F	1	2	At midspan	Between ext. beams E and F
G	2	2	Back-to-back at midspan	Between int. beams D and E
H	1	2	At midspan	As close to barrier as possible
I	1	2	Over controlled joint slab	As close to barrier as possible
J	2	2	Back-to-back at midspan	As close to barrier as possible
K	2	1 and 2	Symmetrically away from controlled joint	Centered over 1st int. beam E
L	1	2	As close to expansion joint as possible	As close to barrier as possible

In a similar way, in Cases C and E one truck was placed straddling Beam E and in Case K two trucks were placed back-to-back straddling Beam E, although the trucks were set at different positions along the span in these other cases. The case shown in Figure 4.9 is the one for which results are presented and discussed herein.

With regard to the other loading positions shown in Table 4.2, it may be seen that several tests were carried out with one or two trucks as close to the barrier as possible. In the last of these cases the truck also was backed up as close as possible into the corner of the span at the controlled joint. These tests were conducted to evaluate the lateral moment performance of the top mat reinforcement supporting the overhang. In this particular bridge, however, the short cantilever length of the overhang and the one-foot-wide Type T202 barrier only allowed the wheel load on the overhang to be centered about 16 inches from the outside edge of the exterior beam's top flange. With this short moment arm the top mat reinforcement was not subjected to much tension and the measured strains were very small. In practice this limitation is expected to be a good thing in that wheel loads in service will never be able to impose very large negative moments on the cantilever. Thus, the key lateral strength requirement of the top mat FRP at each cantilever will come from barrier crash tests recently conducted at Texas A&M University.

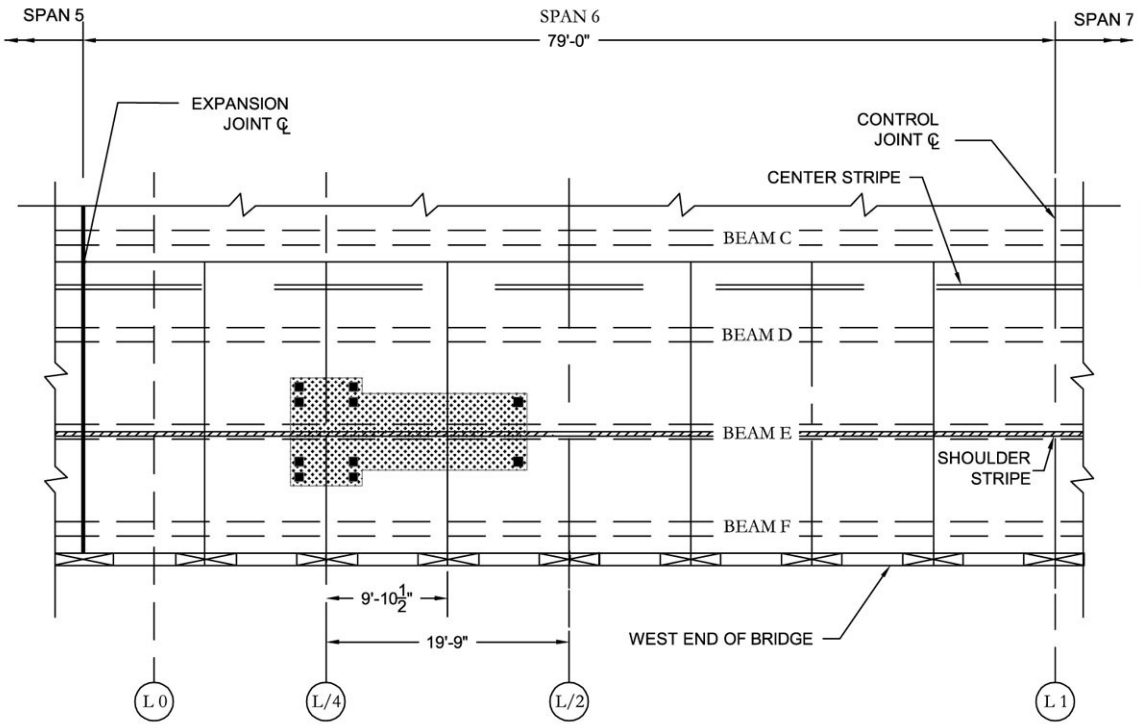

Figure 4.9 Truck Placement for Live Load Test Case D in Span 6

4.6.2 Strain Gauge Results for Load Case D

The key strain measurement in the loading configuration of Figure 4.9 (Case D, shown for Span 6) was in the laterally oriented gauge embedded at the top mat level at the L/4 position along the length. The tires of the rear axles of the truck were centered over this location. The strain in this gauge was measured to be 8.1 x 10^{-6} in/in, or 8.1 μ (microstrains).

In order to calculate the strain expected in this gauge in this test, several assumptions were made and several steps were carried out. First, it was assumed that the loads from the front axle of the truck were far enough away not to cause strain in the subject gauge. Second, a moment distribution was carried out to determine the lateral moment diagram from one edge of the deck to the other, due to the rear axle loads, with particular interest in the negative moment over beam E. The lateral beam-to-slab connections were assumed to be pins in this calculation, and the negative moment over beam E was found to be 19.3 kip-ft. Next, the length of the slab that would resist this moment was estimated by assuming that the rear axle loads would "propagate to Beam E" as shown in Figure 4.10, that is, at a 30-degree angle to the outside from the center of each pair of wheels to the centerline of the beam.

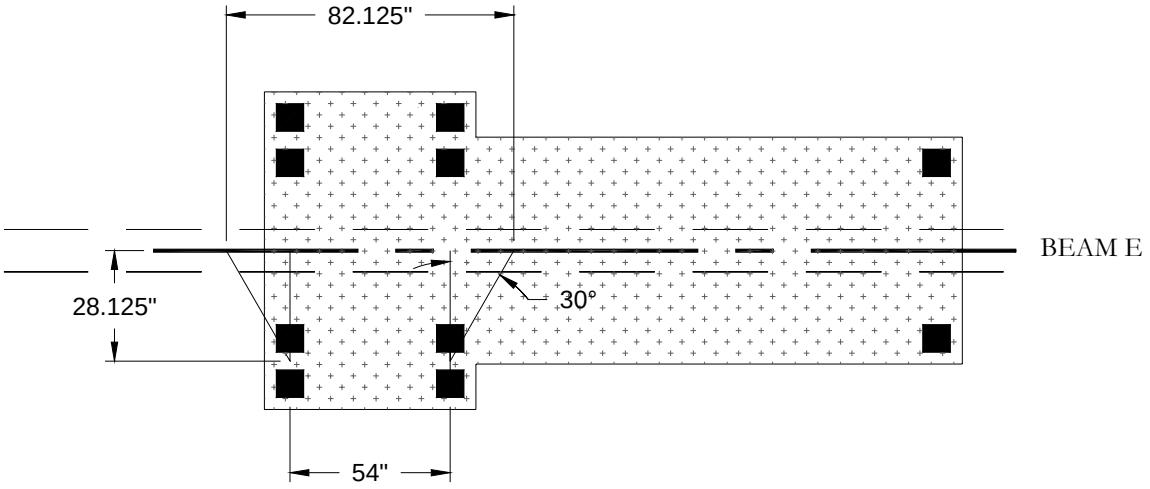

Figure 4.10 Load Propagation from Rear Wheels to Beam E at a 30° Angle

This was a rather arbitrary assumption and could cause a large error in the strain estimate. This assumption meant that an 82.1-inch (6.84-foot) length of the slab would resist the moment over the beam. The resulting average negative moment in the slab per foot along the length of the beam was 19.3 kip-ft/6.84 ft = 2.82 kip-ft/ft.

Next, it was necessary to determine if the calculated moment would cause cracking in the slab, since a cracked section moment of inertia would have to be used if so. The total depth of the slab and the height of the FRP bars in the slab for Span 6 were measured on the bridge during placement of the concrete, and the results are shown in Figure 4.11.

Taking into account the stiffnesses of the concrete and the No. 6 FRP bars in Span 6, the uncracked or gross moment of inertia was found to be 724 in^4. Once the gross moment of inertia was determined, the cracking moment was calculated from the following equation:

$$M_{CR} = \frac{f_r I_g}{y_t} \qquad [4\text{-}1]$$

where

M_{CR} = the cracking moment;
f_r = the cracking stress;
I_g = the gross moment of inertia; and
y_t = the distance from the centroid to the extreme tension fiber.

The cracking stress, f_r, is defined in ACI 318-95 (ACI, 1995) as

$$f_r = 7.5\sqrt{f_c'} \qquad [4\text{-}2]$$

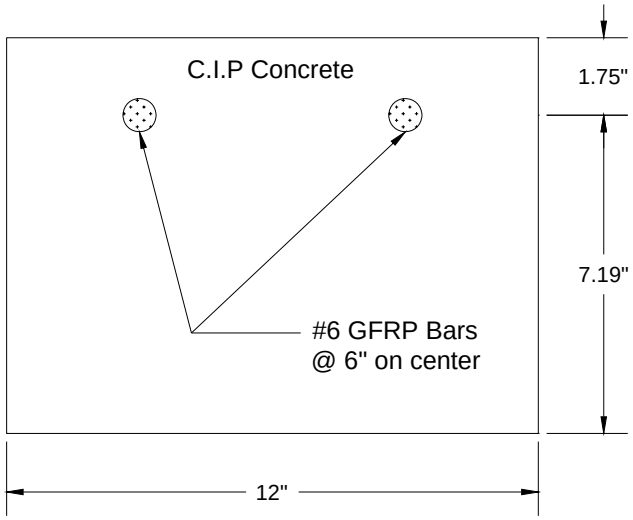

Figure 4.11 One-foot Transverse Deck Section over Beam E in Span 6

where f_c' is the compressive strength of the concrete. Taking f_c' to be 6,000 psi produced a value of f_r of 581 psi. Finally, with y_t equal to 4.47 inches to the top extreme fiber in Figure 4.11, the cracking moment was found to be 7.84 k-ft for a one-foot section of the FRP deck. Since this moment easily exceeded the applied moment of 2.82 k-ft/ft, the bridge deck was not expected to crack under the Case D loading (and it did not). Also, as the cracking moment was greater than the applied moment, the moment of inertia of the slab was taken to be the gross moment of inertia.

The next steps were to determine the stress and then the strain at the level of the top mat due to the average moment of 2.82 k-ft/ft. The stress was found from

$$f = \frac{My}{I_g} \qquad [4\text{-}3]$$

with y = 2.72 inches at the top mat and I_g = 724 in^4 for a one-foot length of the FRP-reinforced slab. This equation yielded a stress of f = 127 psi. For the corresponding strain, the modulus of elasticity of the concrete, E_c, was found from the equation

$$E_c = 57000\sqrt{f'_c} \qquad [4\text{-}4]$$

giving a value of 4.415 ×10^6 psi for 6,000-psi concrete. Finally, then, the calculated strain at the level of the top mat (and the embedded gauge of interest) was

$$\varepsilon = f/E_c = (127 \text{ psi})/(4.415 \text{ x } \times 10^6 \text{ psi}) = 28.8 \ \mu \qquad [4\text{-}5]$$

This estimated strain was over three times the measured strain of 8.1 μ. Perhaps a longer length of the slab should have been assumed to resist the applied moment, especially considering the stiffening effect of the barrier on the behavior of the cantilever. However,

three times the assumed length would not seem to be reasonable. Once again, the final slab thickness may have been greater than even the measured value of 8.94 inches used in this computation, and such an increase could easily reduce the strain at the top mat level.

In any case, the types of strain measurement obtained in the load tests of December, 2001, can be repeated in the future and the long-term performance of both the FRP- and the ECS-reinforced decks of the Sierrita de la Cruz Creek bridge can be judged by comparison to these short-term results.

4.7 Corrosion and Other Long-Term Performance Results

As indicated in the introduction, one of the aims of this research was to provide for different means to evaluate the durability of the FRP-reinforced decks in Spans 6 and 7 in comparison to the other ECS-reinforced decks, in particular those in Spans 1 and 2. Since the main advantage of FRP reinforcement is known to be the fact that it does not corrode, a plan for long-term corrosion monitoring was implemented. On the other hand, there are possible negative performance characteristics of FRP bars in concrete over time, and the research design also provided for the possibility of later extraction and examination of "witness bars" to study these characteristics from time to time. This work will be subject to continued interest by TxDOT.

4.7.1 Corrosion Monitoring

Two different approaches were planned for corrosion monitoring in the instrumented decks. In the first approach 20-foot black steel reinforcing bars were placed in Spans 2 and 6 during Phase I as shown in Figures 3.11, 3.12, and 3.13, with lead wires attached and extended to the under side of the bridge. These bars not only extended over a wide portion of the deck but were bent up into the barriers so as to experience the corrosive effects of de-icing salts washing through the deck-to-barrier joints. The second approach to future corrosion monitoring consisted of including "witness bars" of both black steel and epoxy-coated steel in a number of groups in Phase I and Phase II so that the bars could be extracted and examined for corrosion effects at various times in the future.

The intent of installing the long "corrosion bars" bars was to allow corrosion testing by the half-cell method and/or the linear polarization method at various times in the future. The half-cell test, which can determine only the probability that corrosion is occurring in a concrete pavement underneath a copper-to-copper sulfate half-cell, is described in ASTM C 876 (ASTM, 1995A). It cannot determine the rate of corrosion. The linear polarization method can determine the rate of corrosion but it requires not only an accurate location of the bar but a smooth, uncracked concrete surface away from edges and joints (Carino, 1997). Thus, there may be problems to overcome in its use on the Sierrita de la Cruz Creek bridge. In particular, the tined surface of the deck would have to be ground smooth where a measurement needed to be taken, and the vicinity would have to be uncracked, whereas the cracking results presented above showed relatively few uncracked areas. Also, the key possible corrosion in the deck-to-barrier zone would not be susceptible to linear potential

measurement because of its proximity to the edge. The linear polarization method is described in ASTM G 15 (ASTM 1995B).

Direct measurement of loss of cross section due to corrosion will be possible when and if the black steel and epoxy-coated steel bars are extracted for examination. The number of sets of these bars in Phase II (see Figure 3.15) is sufficient to perform extractions of both types of bars up to nine times from each end of the bridge in the future. Similar sets of bars in Phase I will double these numbers. While the corrosion of these bars is not expected to be affected by being in the FRP- or the ECS-reinforced portion of the bridge, the bars could behave differently because of their locations in the overhang, in the center of a span, or over a controlled joint.

4.7.2 FRP Bar Performance

While GFRP bars are known to be inert to chlorides and other chemicals, the glass fibers are susceptible to moisture and other possible effects. Extraction of the GFRP bars along with their companion black steel and ECS bars at different intervals in the future would allow for useful studies of how the GFRP bars are performing. The bars are not long enough to be used in tensile tests since special grips requiring a rather long specimen are needed. However, examination of the ends of the bars where moisture and chemicals can reach the glass fibers could be revealing, and the general condition of the protective matrix should also be checked. It is suggested that bars from the overhang, the centers of the spans, and the controlled joints be extracted and examined at least three times in the future, say three, ten, and thirty years after the bridge's construction.

CHAPTER 5. SUMMARY, CONCLUSIONS, AND SUGGESTED FUTURE RESEARCH

5. 1 Summary of Instrumentation and Measurements

Several types of instrumentation were employed on the Sierrita de la Cruz Creek bridge for comparison of the performance of the GFRP-reinforced concrete decks in Spans 6 and 7 to that of the decks in the other spans, which were reinforced with epoxy-coated steel (ECS). The different types of instrumentation and measurement already installed and utilized included: 1) temperature measurements with thermocouples embedded in the deck; 2) displacements of the cantilevered edges of the deck relative to the exterior beams from displacement transducers (LVDT's) mounted on the beams (although these measurements were unsuccessful); 3) total station (surveying) measurements of the deflections at the centers of key spans; 4) strains from strain gauges embedded in the deck and attached to the surfaces of the deck and its supporting prestressed concrete beams; and 5) extensive crack mapping on two matching FRP- and ECS-reinforced spans. Any of these types of measurement can be repeated in the future to evaluate the long-term behavior of the two types of deck reinforcement. Of course, new displacement gauges will have to be installed on the exterior beams for the deck edge displacement measurements, and only those strain gauges indicated as still operable in Appendix D will provide new data, although some new exterior strain gauges could be installed. Besides the types of measurements already made, black steel "corrosion bars" were installed in the decks for future corrosion probability and corrosion rate measurements, and black steel, ECS, and GFRP "witness bars" were installed near the top surface for extraction at intervals in the future so that the conditions of these three types of rebar can be examined and compared. The sections below summarize the results of the tests conducted so far and draw several important conclusions.

5.2 Temperatures During Casting

Temperatures were measured within the cast-in-place concrete around and over one precast panel for several days during the Phase I and Phase II deck pours. During Phase II construction of Span 6 the temperature rose from approximately 21^{o}C (70^{o}F) to a maximum of 39^{o}C (102^{o}F) due to the heat of hydration and with under-slab heating applied due to the cold ambient temperatures. This maximum occurred near mid-depth of the 8-inch-thick deck and was measured 24 hours after the concrete was placed over the thermocouples. It was slightly below the lowest temperatures at which the tensile strength of GFRP has been observed to be reduced (Nishizaki and Meiarashi, 2002).

5.3 Deck Cracking

The cracks in the upper surfaces of the Phase II decks in Spans 2 and 6 were carefully mapped 13 months after their construction. Mapping was done both before and during a series of live load tests. The various live load test cases are detailed in Appendix C. The cracking was very similar in the two differently reinforced spans, although one longitudinal crack over the third interior beam appeared in the FRP-reinforced Span 6 and not in the ECS- reinforced

Span 2. All of the cracks were attributed to temperature and shrinkage effects as they did not widen or elongate under the imposed live loads. The longitudinal crack in Span 6 appeared to be caused by extra shrinkage in the entirely cast-in-place middle bay of the bridge as compared to the shrinkage in the bays with 4-inch-thick precast panels. The lack of occurrence of a similar crack in Span 2 could have been affected by any number of factors: a difference in concrete mixes, in ambient temperatures during placement, in underneath heating, in the ECS vs. FRP stiffnesses in the top mat, or in diminished bond properties of the GFRP.

5.4 Displacements

The intended deck-edge displacement measurements during the main live load tests of December, 2001, failed to materialize because of a malfunction of the one data acquisition system module allocated to these measurements. However, small displacements at the centers of Spans 2 and 6 due to one- and two-truck live loads in September, 2002, proved to agree fairly well with calculated values. The measured displacements were somewhat smaller than the theoretical ones, which may have been due to a lack of precision, a difference in moduli of the supporting beams, unaccounted influence of the railings, or a thicker final deck slab than the assumed 8-inch-thick slab.

5.5 Strains

A number of the many strain gauges installed in the deck and on the beams of the bridge also failed to provide useful data during the December, 2001, live load tests. These failures were attributed to vandalism, possible damage from workers walking over the mat, and a malfunction in one of the seven data acquisition system modules allocated to strains. Nevertheless, some useful strain data were obtained, and an example analysis is presented in Section 4.6. In this example the measured strain was somewhat smaller than the calculated strain. This result, like that for the measured vs. calculated deflections, could be due to a thicker than expected slab and/or the resistance of a longer than assumed length of the slab participating in resisting the applied moment.

5.6 Recommended Long-Term Performance Monitoring

Results of tests on the Sierrita de la Cruz Creek bridge deck so far are very encouraging. They have shown no problems with surface cracking or stiffness. Therefore, significant long-term deterioration is not expected. However, should TxDOT decide to monitor this bridge to assess its long-term behavior, such monitoring will be possible.

The instrumentation of the bridge that has been set up by Texas Tech University should allow for a variety of tests to monitor and evaluate the long-term performance of both the FRP- and ECS-reinforced portions of the bridge. First, tests of the type already performed, including crack mapping and strain and displacement measurements under calibrated live loading, can be repeated from time to time over the long term. A summary of the gauges that are still usable is presented in Appendix D. Also, tests not yet performed can be conducted at appropriate intervals, especially corrosion tests on the black steel “corrosion bars” installed

for this purpose, and possible extraction of the black steel, ECS, and FRP “witness bars” to see what moisture, age, cyclic loading, weather, de-icing, and other effects may have had on these three types of reinforcing bars. Enough witness bars have been installed (and their locations accurately documented in Appendices A and B) for extraction of all three types from different parts of the bridge at three to six different times in the future.

REFERENCES

ACI (1995). Building Code Requirements for Structural Concrete (ACI 318-95). American Concrete Institute. Farmington Hills, MI.

ACI 440 (2001). *Guide for the Design and Construction of Concrete Reinforced with FRP Bars* (pp. 6-12). American Concrete Institute: Farmington Hills.

ASTM (1995A). Standard C 876: Test Method for Half-Cell Potential of Uncoated Reinforcing Steel in Concrete. *1995 Annual Book of ASTM Standards, Vol. 04.02.*

ASTM (1995B). Standard G 15: Terminology Relating to Corrosion and Corrosion Testing. *1995 Annual Book of Standards, Vol. 03.02.*

Bakht, B., Al-Bazi, G., Banthia, N. (2000). Canadian Bridge Design Code Provisions for Fiber-Reinforced Structures. *Journal of Composites for Construction. 4(1),* 3-10.

Bradberry. T. (2001). Concrete Bridge Decks Reinforced with Fiber-Reinforced Polymer Bars. *Transportation Research Record 1770,* 94-104.

Carino, N. (1997). Nondestructive Test Methods. In E. Nawy (Ed.), *Concrete Construction Engineering Handbook* (pp. 51-56). New York: CRC Press.

Cosenza, E., Manfredi, G., Realfonzo, R. (1997). Behavior and Modeling of Bond of FRP Rebars to Concrete. *Journal of Composites for Construction, 1(2),* 40-51.

Gentry, T.,and Husain, M. (1999). Thermal Compatibilty of Concrete and Composite Reinforcements. *Journal of Composites for Construction, 3(2),* 82-86.

Hastak, M., and Halpin, D. (2000). Assessment of Life-Cycle Benefit-Cost of Composites in Construction. *Journal of Composites for Construction, 4(3),* 103-111.

Hughes Brothers. (2002). Mechanical Properties of GFRP Rebar. *http://www.hughesbros.com/RebarMech.html*.

Katz, A. (1998). Effect of Helical Wrapping on Fatigue Resistance of GFRP. *Journal of Composites for Construction, 2(3),* 121-125.

Katz, A., Berman, N., and Bank, L. C. (1999). Effect of High Temperature on Bond Strength of FRP Rebars. *Journal of Composites for Construction, 3(2),* 73-81.

Katz, A. (2000). Bond to Concrete of FRP Rebars After Cyclic Loading. *Journal of Composites for Construction, 4(3),* 137-144.

National Instruments (2002). Strain Gauge Measurement—A Tutorial. *http://zone.ni.com/devzone/conceptd.nsf/webmain/C83E9B93DE714DB086256866007 04DB1?OpenDocument.*

Nishizaki, I., and Meiarashi, S. (2002). Long-Term Deterioration of GFRP in Water and Moist Environment. *Journal of Composites for Construction, 6(1),* 21-27.

Phelan, R. (1993). *High Performance Maglev Guideway Design*. (pp. 89-90). Massachusetts Institute of Technology: Cambridge.

Riggs, D., Schuford, R., and Lewis, R. (1982). Graphite Fibers and Composites. In G. Lubin (Ed.), *Handbook of Composites* (pp. 196-272). New York: Van Norstrand Reinhold Company.

Soroushian, P., Ravanbakhsh, S., and Drzal, L.T. (2001). Non-Metallic Reinforcement of Concrete Bridge Decks. *Report RC 1392*. Lansing: Michigan Department of Transportation.

APPENDIX A

PHASE I INSTRUMENTATION PLANS

APPENDIX A

PHASE I INSTRUMENTATION PLANS

The following figures, with sheet numbers FRP 0001 through 0020 in the lower right-hand part of the title block, provide drawings of the instrument locations and configurations for the first phase construction, that is, the northbound lanes for which the pour occurred on July 24 and 25, 2000.

The first page, called the Title Page, shows a table of contents for this appendix, but a few comments may help the reader in following the drawings. Sheet 0002 shows the two phases of construction. The Legend on the right-hand side of the Title Page shows the symbols used for the six categories of instruments that were installed. General locations for the strain gages, thermocouples, LVDT's, and witness bars on the plans are shown with unique symbols. Furthermore, in the sections and detail drawings the longitudinal and lateral strain gages are given special symbols.

The first set of drawings has a general plan as a main drawing and is followed by sections and details that pertain to it. For example, for the FRP-reinforced Span 6:

- The general plan is shown on Sheet 0003, with the locations of Sections A, B, and C and Details 1, 2, and 3 indicated.
- Sheets 0004, 0005, and 0006 show Sections A, B, and C, respectively, with strain gages.
- Sheet 0007 shows Detail 1, again from Sheet 0003, an isometric of the thermocouples.
- Sheet 0008 shows Details 2 and 3, close-up plans of witness bars at two locations.
- Sheets 0009, 0010, and 0011 show Sections D, E, and F from Sheet 0008, with witness bar details.

The second set of drawings gives detailed dimensions to the instruments and to the framing bars around the witness bars.

- The general plan for Spans 1 and 2 is shown on Sheet 0012, with the key dimensions to the centers of all of the witness bar groups, the only instrumentation installed there. The detailed dimensions for the overhang witness bars are shown on this sheet, and the detailed dimensions for the witness bars over Beam B are shown on Sheet 0013.
- Similarly, the general plan for Spans 6 and 7 is shown on Sheet 0014, with the key dimensions to the centers of all of the witness bar groups. However, corrosion bars and strain gages were also installed in these spans, and Sheets 0015 and 0016 give detailed dimensions for the instruments over Beam B and those in the overhang witness, respectively.
- Sheets 0017, 0018, and 0019 show the arrangements of, and the dimensions to, the framing bars installed around the various sets of witness bars. These are indicated as Details 4, 5, and 6 on Sheets 0012 and 0014.

Finally, Sheet 0020 shows Sections H from Sheet 0019, indicating how all of the witness bars were supported above the top mat of the slab reinforcement (and with minimum cover) so that they could be extracted easily without clipping the main reinforcement.

APPENDIX B

PHASE II INSTRUMENTATION PLANS

APPENDIX B

PHASE II INSTRUMENTATION PLANS

The following figures, with sheet numbers FRP 0021 through 0039 in the lower right-hand part of the title block, provide drawings of the instrument locations and configurations for the second phase construction, that is, the southbound lanes for which the pour occurred on November 15 and 16, 2000.

The first page, called the Title Page, shows a table of contents for this appendix, and again a few comments may help the reader in following the drawings. Sheet 0022 highlights the Phase II instrumentation regions. The Legend on the right-hand side of the Title Page shows only special symbols for the strain gages. In this appendix only the locations of strain gauges and witness bars (this time shown with straight lines) are documented.

The first set of drawings has general plans for the ECS-reinforced Spans 1 and 2 and for the FRP-reinforced Spans 6 and 7 as main drawings, followed by sections and details that pertain to these drawings:

- The general plans are shown on Sheet 0023 for Spans 1 and 2 and on Sheet 024 for Spans 6 and 7, with the locations of Sections I, J, and K and Details 7 through 18 indicated (not all on either sheet).
- Sheets 0025, 0026 and 0027 show Sections I, J, and K, respectively, with witness bar arrangements.
- Sheet 0028 and 0029 show Details 7 and 8, respectively, with framing bars at the continuity slab and the overhang.
- Sheet 0030 shows Details 9-11 (mirror images of 12-14) and Details 15-16 (mirror images of 17-18).

A second set of drawings gives detailed dimensions to the strain gauges in Spans 2 and 6:

- The general plans are shown on Sheet 0031 for Span 2 and on Sheet 0032 for Span 6, with the locations of the three Sections L, the one Section M, and Details 19 through 56 indicated (not all on either sheet).
- Sheets 0033 and 0034 shows Sections L and M, respectively, with dimensions to surface and embedded gauges and further sections 57 through 61 indicated.
- Sheet 0035 shows the depths of various embedded strain gauges in Details 57 through 61.
- Sheet 0036 shows details of the locations in plan of strain gauges at sections L0, L1, L/4 and L/2.
- Sheets 0037 through 0039 show details 19-30, 31-38, 39-50, and 51-56, illustrating embedded strain gauge cover dimensions.

APPENDIX C

LIVE LOAD TEST CASES

APPENDIX C

LIVE LOAD TEST CASES

The live load test series conducted on December 12 and 13, 2001, envisioned 12 different loading cases, that is, different positions of calibrated trucks (one or two) on the Phase II (west) side of the Sierrita de la Cruz Creek bridge. Tests were carried out on both the FRP-reinforced and the ECS-reinforced spans, and the cracking prior to any loading was also mapped in both instances. This appendix shows sketches of the 12 truck positions considered, designated as Cases A through L, although the numbering of the pages does not always follow alphabetic order. Also, in a few of the cases more than one test was conducted (usually with the truck or trucks on the overhang, but closer and closer to the barrier). The sequential test number(s) corresponding to each case are shown in parentheses after the case letter. For example, A(5) indicates that Case A was the fifth test actually performed. The sequence number for each test corresponded to its position in the computer files and its correspondence with the case letter had to be preserved.

For some of the tests no crack mapping was conducted. For those that included crack mapping the specific subsections of the mapping area that were examined during the live loading are shown in figures accompanying those cases. In only one instance was a new crack detected.

The figures show designations such as I.1(a) and II.2(a), which can be ignored.

Brief descriptions of the cases are presented in Table 4.1 of the main text. The tables below give a roadmap to the following drawings for the various tests.

A. Loading of FRP-reinforced Spans 6 and 7: Initial Cracking Shown in Figure 0043

Test Sequence No.	Test Case	Loading Figure No.	Crack Mapping Figure No.
1	B	0044	-
2	C	0045	-
3	D	0046	-
4	E	0047	-
5	A	0048	-
6	F	0049	-
7-8	H	0050	0051
9	Hi	0052	0054
10	Hii	0053	0054
11-12	I	0055	0056
13-14	J	0057	0058
15	L	0059	0060
16	G	0061	0062
17	K	0063	0064

B. Loading of ECS-reinforced Spans 1 and 2: Initial Cracking Shown in Figure 0065

Test Sequence No.	Test Case	Loading Figure No.	Crack Mapping Figure No.
18	B	0066	-
19	A	0067	-
20	C	0068	-
21	D	0069	-
22	E	0070	-
23	L	0071	0072
24	F	0073	-
25	J	0074	0075
26	K	0076	0077
27	G	0078	0079

Sheet 0051 shows the only “new” crack found during the entire set of load tests. However, with its measured width of 0.006 inches it was not considered to be significant. It is also possible that the crack was overlooked during the initial crack mapping shown on Sheet 0043.

A comparison of the initial crack patterns in Spans 1 and 2, shown on Sheet 0065 for the ECS reinforcing mat, and the initial crack patterns in Spans 6 and 7, shown on Sheet 0043 for the FRP reinforcing mat, is intuitive. All cracks were small and were considered to be induced by temperature and shrinkage. The only major difference observed was the presence of a longitudinal crack in the FRP-reinforced span. A second set of live load tests was performed to determine if this crack would widen under load. Results were negative, leading to the conclusion that this crack was also induced by temperature and shrinkage.

APPENDIX D

STRAIN AND DISPLACEMENT GAUGE ASSESSMENT

APPENDIX D

STRAIN AND DISPLACEMENT GAUGE ASSESSMENT

The strain gauge and displacement gauge instrumentation installed on the Sierrita de la Cruz bridge was evaluated in January of 2004 to document its potential for future load testing of the bridge. Investigators tested the status of all of the strain gauges at the junction boxes in the two instrumented spans, Span 6 with FRP reinforcement and Span 2 with ECS reinforcement. The LVDT setups that were installed in December 2001 were also observed and evaluated. Based on these assessments, investigators made the recommendations for future testing given at the end of this Appendix.

D.1 Strain Gauges

The strain gauges installed in the FRP-reinforced span (Span 6) were tested for functionality using a Micro-Measurements strain indicator and for continuity using a multimeter. A multimeter is an instrument capable of measuring multiple types of electrical behavior, specifically resistance, voltage, and amperage (current). Strain gauges in the steel-reinforced span (Span 2) were tested for continuity only, as the junction box for this span is high above the ground and holding the strain indicator and connecting each set of leads to it was too awkward an operation to perform on a tall ladder. The strain gauges were then classified as either working, having full continuity, having partial (Red-Black or Red-White) continuity, unsteady, not working, having an unknown location, or not wired up. A description of each of these functionality classifications is given in Table D.1, along with the number of gauges in each class for each span. If a gauge in the FRP span showed to be working with the strain indicator, continuity readings were not performed with the multimeter. For the ECS span, however, only continuity was checked, but so many of the gauges had their lead wire labels pulled off by vandals that most of the gauges had to be classified as having an "unknown location," anyway.

It is believed that not only the "working" gauges but those with full or partial continuity can be used in future load tests. Gauges which have partial continuity are likely to be recoverable by repairing the splices between the gauges and their lead wires. Even those classified as "unsteady" are also considered to be recoverable with similar upgrading.

Table D.1 shows that plenty of working or at least potentially usable gauges exist in the FRP span (62 of 84 or almost 75 percent are "working," 3 more have full continuity, and 4 others are expected to be recoverable as they have either Red-Black or Red-White continuity). On the other hand, very few of the gauges are usable in the ECS span (only 12 of 88 gauges or 14 percent have a known location and are working). Thus, while a comparison in behavior between the two spans would be desirable, future load tests should probably be aimed at the FRP span.

Detailed records of the individual gauges and each one's status are given in Table D.2 and Drawings 89 through 93 for the FRP-reinforced Span 6. Corresponding data are given in Table D.3 and Drawings 84 through 88 for the ECS-reinforced Span 2. The individual gauges are identified by the six-space labeling system shown in Drawing 83.

Basically, the six pieces of information in each label give the longitudinal cross-section in which the gauge is located,

Table D.1. Strain Gauge Functionality Classifications

Label	Description	# in FRP Span	# in ECS Span
Working	The gauge is working and giving constant strain readings on the strain indicator	62	Not Measured
Full Continuity	No reading on the strain indicator but both Red-Black and Red-White continuity on the multimeter	3	12
RB Continuity	No reading on the strain indicator but Red-Black continuity on the multimeter	0	0
RW Continuity	No reading on the strain indicator but Red-White continuity on the multimeter	2	2
Unsteady	A strain reading was observed on the strain indicator but did not hold a constant value	2	Not Measured
Not Working	No reading on the strain indicator and no continuity on the multimeter	10	1
Unknown Location	Unlabeled wires could not be distinguished from other wires	1	64
Not Wired Up	No leads are connected to the junction box	4	9

whether the gauge is over a beam or panel, the vertical position of the gauge, whether the gauge is an embedded or surface-mounted gauge, whether the gauge is oriented longitudinally or transversely with respect to the length of the bridge, and the number of the beam or panel on which the gauge is centered, starting from the outside beam of Phase II. Drawing 84 shows in plan view the gauges along each longitudinal cross-section in Span 2 and Drawing 89 shows the same information for Span 6. The drawings following each of these plan views illustrate the individual gauge locations in section views at each cross-section. These drawings also indicate the status of each gauge, with clear shading showing a working gauge, gray shading showing an unknown location gauge, and black shading showing a gauge that is not working or not wire up.

The numbers and letters in the columns headed as “Box Label” in Tables D.2 and D.3 represent the terminals within the junction boxes to which the gauge lead wires are attached. A schematic of the rows of terminals in each junction box is shown in Drawing 83. Junction box numbers 1 through 33 were used to label terminals for surface-mounted strain gauges and junction box letters were used to label terminals for embedded strain gauges. A few terminals in each box were wired up but not labeled at all. There seems to be no explanation why data from terminal 33 were not reported in Tables D.2 and D.3; apparently the terminals simply were skipped in the evaluation exercise.

Table D.2. FRP-Reinforced Span Gauge Functionality

Box Label	Gauge	Status	Box Label	Gauge	Status	Box Label	Gauge	Status
1	L/2-PTST-5	working	A	0L-BBSA-2	unsteady	GG	L/2-PMEA-5	working
2	L/2-PTSA-5	not working	B	0L-BMET-6	working	HH	L/2-BMET-4	working
3	L/2-PTST-3	Full continuity	C	0L-BMEA-6	working	II	L/2-BMEA-4	unsteady
4	L/2-PTSA-3	not working	D	0L-BTEA-6	working	JJ	L/2-BTEA-4	working
5	L/4-PTST-5	working	E	0L-PMET-5	working	KK	L/2-PMET-3	working
6	L/4-PTSA-5	working	F	0L-PMEA-5	working	LL	L/2-PMEA-3	working
7	L/4-PTST-3	Full continuity	G	0L-BMET-4	working	MM	L/2-BMET-2	working
8	L/4-PTSA-3	not working	H	0L-BMEA-4	working	NN	L/2-BMEA-2	Full continuity
9	0L-PTST-5	working	I	0L-BTEA-4	working	OO	L/2-BTEA-2	Not wired up
10	0L-PTSA-5	working	J	0L-PMET-3	working	PP	L/2-OHET-1	working
11	0L-PTST-3	working	K	0L-PMEA-3	working	A1	Controlled joint	working
12	0L-PTSA-3	not working	L	0L-BMET-2	working	B1	Controlled joint	working
13	L/2-BBSA-6	Not wired up	M	0L-BMEA-2	working	C1	Controlled joint	working
14	L/2-PBST-5	working	N	0L-BTEA-2	working	D1	Controlled joint	working
15	L/2-PBSA-5	working	O	0L-OHET-1	working	A2	Controlled joint	not working
16	L/2-BBSA-4	working	P	L/4-BMET-6	working	B2	Controlled joint	not working
17	L/2-PBST-3	Not wired up	Q	L/4-BMEA-6	working	C2	Controlled joint	not working
18	L/2-PBSA-3	working	R	L/4-BTEA-6	working	D2	Controlled joint	not working
19	L/2-BBSA-2	working	S	L/4-PMET-5	working		L/2 BTEA-6	working
20	L/4-BBSA-6	Not wired up	T	L/4-PMEA-5	working		L/2 OHES-1	working
21	L/4-PBST-5	RW continuity	U	L/4-BMET-4	working			
22	L/4-PBSA-5	working	V	L/4-BMEA-4	working			
23	L/4-BBSA-4	not working	W	L/4-BTEA-4	working			
24	L/4-PBST-3	working	X	L/4-PMET-3	working			
25	L/4-PBSA-3	working	Y	L/4-PMEA-3	working			
26	L/4-BBSA-2	working	Z	L/4-BMET-2	working			
27	0L-BBSA-6	working	AA	L/4-BMEA-2	working			
28	0L-PBST-5	working	BB	L/4-BTEA-2	working			
29	0L-PBSA-5	working	CC	L/4-OHET-1	working			
30	0L-BBSA-4	not working	DD	L/2-BMEA-6	working			
31	0L-PBST-3	working	EE	L/2-PMET-5	working			
32	0L-PBSA-3	RW continuity	FF	Unknown	(working)			

Note: Color Scheme:

Color	Classification
Green	Working
Blue	Continuity or Unsteady
Red	Not Working
Orange	Unknown Location
Yellow	Not Wire Up

Table D.3. ECS-Reinforced Span Gauge Functionality

Box Label	Gauge	Status	Box Label	Location	Status	Box Label	Location	Status
1	Unknown	Full continuity	A	Unknown	Full continuity	GG	Unknown	Full continuity
2	Unknown	not working	B	Unknown	Full continuity	HH	Unknown	Full continuity
3	Unknown	not working	C	Unknown	Full continuity	II	Unknown	not working
4	Unknown	Full continuity	D	Unknown	not working	JJ	Unknown	Full continuity
5	Unknown	Full continuity	E	Unknown	not working	KK	Unknown	Full continuity
6		Not wired up	F	Unknown	Full continuity	LL	Unknown	Full continuity
7		Not wired up	G	Unknown	RB continuity	MM	Unknown	Full continuity
8	Unknown	Full continuity	H	Unknown	RB continuity	NN	Unknown	Full continuity
9	Unknown	Full continuity	I	Unknown	Full continuity	OO	Unknown	Full continuity
10		Not wired up	J	Unknown	RB continuity	PP	Unknown	not working
11		Not wired up	K	Unknown	not working	A1	Unknown	Full continuity
12		Not wired up	L	Unknown	Full continuity	B1	Unknown	Full continuity
13		Not wired up	M	Unknown	Full continuity	C1	Unknown	Full continuity
14	0L-PBSA-5	Full continuity	N	Unknown	not working	D1	Unknown	not working
15	0L-PBST-5	not working	O	Unknown	not working	A2	Unknown	Full continuity
16	0L-BBSA-4	Full continuity	P	Unknown	Full continuity	B2	Unknown	Full continuity
17	0L-BBSA-3	Full continuity	Q	Unknown	Full continuity	C2		Not wired up
18	Unknown	Full continuity	R	Unknown	RW continuity	D2	Unknown	not working
19	0L-BBSA-2	Full continuity	S	Unknown	Full continuity		Unknown	Full continuity
20	Unknown	not working	T	Unknown	not working		Unknown	not working
21	L/4-PBSA-5	Full continuity	U	Unknown	not working		Unknown	not working
22	L/4-PBST-5	Full continuity	V	Unknown	Full continuity		Unknown	not working
23	L/4-BBSA-4	RW continuity	W	Unknown	Full continuity		Unknown	not working
24	L/4-PBSA-3	Full continuity	X	Unknown	not working		Unknown	not working
25	L/4-PBST-3	Full continuity	Y	Unknown	not working			
26	L/2-BBSA-6	Full continuity	Z	Unknown	Full continuity			
27	L/2-PBSA-5	Full continuity	AA	Unknown	Full continuity			
28		Not wired up	BB	Unknown	not working			
29		Not wired up	CC	Unknown	Full continuity			
30	L/2-PBSA-3	Full continuity	DD	Unknown	not working			
31	L/2-PBST-3	RW continuity	EE	Unknown	not working			
32	L/2-BBSA-2	Full continuity	FF	Unknown	not working			

Note: Color Scheme:

Color	Classification
Blue	Continuity or Unsteady
Red	Not Working
Orange	Unknown Location
Yellow	Not Wire Up

Figure D.1 LVDT Mounting Brackets on Span 6

D.2 Displacement Gauges

Brackets for mounting LVDT s at the edges of the Phase II overhang are still in place and available for future deflection measurements. The current state of the brackets is shown in Figure D.1**.**

D.3 Recommendations for Protection and Future Monitoring of the Instrumentation

Investigators at the bridge in January of 2004 also noted that there were lateral cracks in the bottom of the cast-in-place overhang at regular intervals of about four feet. These cracks show up as white lines in Figure D.1. Continuation of each crack was observed to extend through the outside edge and across the top of the overhang, indicating that it was a full-depth crack.

Based on the assessment of the investigators, it is expected that a certain amount of work should be performed in order for future monitoring of the strain gauges to be effective. The recommendations of the investigators are as follows:

- All lead wire splices should be replaced and heat shrunk.
- All lead wires should be passed through conduits underneath the bridge for protection from vandals.
- All leads should be soldered in order to eliminate the small fluctuations in resistance that can occur when the wires are not soldered.
- For tests on the steel span, several exterior strain gauges should be replaced.